

Original Article

Cite this article: De Min A, Velicogna M, Ziberna L, Chiaradia M, Alberti A, and Marzoli A (2020) Triassic magmatism in the European Southern Alps as an early phase of Pangea break-up. *Geological Magazine* **157**: 1800–1822. <https://doi.org/10.1017/S0016756820000084>

Received: 9 May 2019
Revised: 29 December 2019
Accepted: 13 January 2020
First published online: 30 April 2020


Keywords:

Dolomites; basalts; Pangea; geodynamic settings

Author for correspondence:

De Min Angelo, Email: demin@units.it

Triassic magmatism in the European Southern Alps as an early phase of Pangea break-up

Angelo De Min¹ , Matteo Velicogna¹, Luca Ziberna^{1,2}, Massimo Chiaradia³, Antonio Alberti¹ and Andrea Marzoli⁴

¹Dipartimento di Matematica e Geoscienze, Università degli Studi di Trieste, Via Weiss 8, 34128 Trieste, Italy; ²Bayerisches Geoinstitut, University of Bayreuth, 95440 Bayreuth, Germany; ³Department of Earth Sciences, University of Geneva, Rue des Maraichers 13, 1205 Geneva, Switzerland and ⁴Dipartimento di Geoscienze, Università di Padova, Via Gradenigo 6, 35131 Padova, Italy

Abstract

Magmatic rocks from the Dolomites, Carnic and Julian Alps, Italy, have been sampled to investigate the origin and geodynamic setting of Triassic magmatism in the Southern Alps. Basaltic, gabbroic and lamprophyric samples have been characterized for their petrography, mineral chemistry, whole-rock major and trace elements, and Sr, Nd and Pb isotopic compositions. Geothermobarometric estimates suggest that the basaltic magmas crystallized mostly at depths of 14–20 km. Isotopic data show variable degrees of crustal contamination decreasing westwards, probably reflecting a progressively more restitic nature of the crust, which has been variably affected by melting during the Permian period. Geochemical and isotopic data suggest that the mantle source was metasomatized by slab-derived fluids. In agreement with previous studies and based on geological evidence, we argue that this metasomatism was not contemporaneous with the Ladinian–Carnian magmatism but was related to previous subduction episodes. The lamprophyres, which likely originated some 20 Ma later by lower degrees of melting and at higher pressures with respect to the basaltic suite, suggest that the mantle source regions of Triassic magmatism in the Dolomites was both laterally and vertically heterogeneous. We conclude that the orogenic signatures of the magmas do not imply any coeval subduction in the surrounding of Adria. We rather suggest that this magmatism is related to the Triassic rifting episodes that affected the western Mediterranean region and that were ultimately connected to the rifting events that caused the break-up of Pangea during the Late Triassic – Early Jurassic period.

1. Introduction

The Middle and Upper Triassic units in the Dolomites, Carnic Alps and Julian Alps (northeastern Italy) include a unique suite of magmatic products, from basalts, gabbroic rocks and lamprophyres to rhyolites, tuffs and minor granitoids. These products could potentially belong to a wider magmatic province, which crops out over a large area in the European Southern and Eastern Alps (Fig. 1) and possibly even in Calabria, Sardinia, northern Apennines and Dinarides (Beccaluva *et al.* 2005). This magmatism has been associated either to compressional, extensional and/or transtensional geodynamics (e.g. Crisci *et al.* 1984; Castellarin *et al.* 1988; Sloman, 1989; Bonadiman *et al.* 1994; Stampfli *et al.* 2002; Armienti *et al.* 2003; Csontos & Vörös, 2004; Beccaluva *et al.* 2005; Doglioni & Carminati, 2008; Schmid *et al.* 2008; Zanetti *et al.* 2013; Abbas *et al.* 2018; Bianchini *et al.* 2018; Casetta *et al.* 2018b; Storck *et al.* 2019). Such contrasting interpretations are probably due to (1) the palaeogeographic position of the outcrops (at the edge between Gondwana and Laurasia), for which palaeogeographic reconstructions are still debated (e.g. Sengör, 1984; Kozur, 1991; von Raumer, 1998; Ziegler & Stampfli, 2001; Nikishin *et al.* 2002; Stampfli & Borel, 2002; Csontos & Vörös, 2004; Golonka, 2004; Bortolotti & Principi, 2005; Muttoni *et al.* 2009; Schettino & Turco, 2011), and (2) the apparent contrast between the extensional to transcurrent tectonics (e.g. Doglioni, 1987; Vai, 1991; Gianolla *et al.* 1998; Bortolotti & Principi, 2005; Beltrando *et al.* 2015) and the apparent orogenic geochemical fingerprints of many of the magmatic products studied so far (e.g. De Vecchi & Sedeà, 1983; Castellarin *et al.* 1988; Sloman, 1989; Gasparotto & Simboli, 1991; Bonadiman *et al.* 1994; Armienti *et al.* 2003; Casetta *et al.* 2018b; Lustrino *et al.* 2019). What gained the interest of the geological community is the fact that this magmatism took place shortly before the break-up of Pangea, in a lithosphere that was previously affected by the Variscan collision and possibly by even older orogenic events. This makes the Triassic magmatism in the Southern Alps an attractive case study that can help to understand lithospheric processes in complex geodynamic settings.

Geochemical and petrographic data about this magmatism have increased over the last decades (e.g. Sloman, 1989; Bonadiman *et al.* 1994; Cassinis *et al.* 2008; Miller *et al.* 2011;

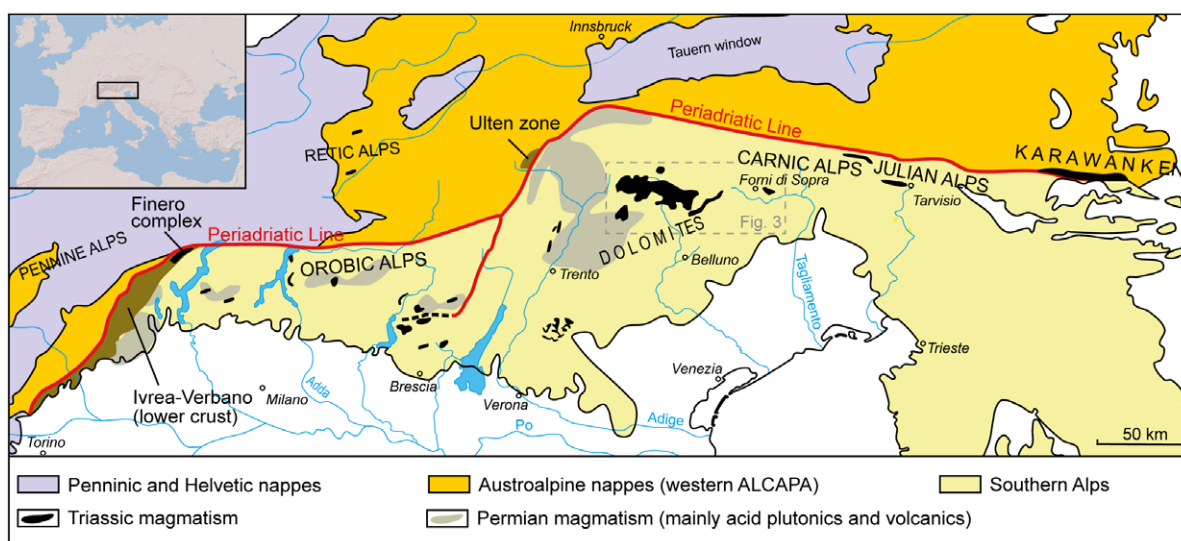


Fig. 1. (Colour online) Geological sketch map of the Southern Alps (modified after Schmid *et al.* 2004) and known locations of Triassic igneous rocks and volcanoclastics (after De Vecchi & Sedeà, 1983; Castellarin *et al.* 1988; Armienti *et al.* 2003; Furrer *et al.* 2008; Zanetti *et al.* 2013; Beltràn-Triviño *et al.* 2016). The location of the exposed lower crust of the Ivrea-Verbano (Handy *et al.* 1999), Variscan Ulten peridotites (Tumiati *et al.* 2003) and main Permian magmatic outcrops (Rottura *et al.* 1998; Schaltegger & Brack, 2007) in the Southern Alps are also shown.

Beltràn-Triviño *et al.* 2016; Bianchini *et al.* 2018; Casetta *et al.* 2018a, b, 2019; Lustrino *et al.* 2019). However, a clear picture of its geodynamic context is hindered by the widespread hydrothermal alteration of the outcrops, the complex palaeogeography and the lack of a comprehensive review of the geology of this area. The aim of this work is to address some of these problems. We present new major- and trace-element and Sr–Nd–Pb isotopic data on carefully sampled and selected Triassic magmatic rocks from the eastern Southern Alps, and combine these with existing data from the neighbouring areas. These data are placed in a broader context by summarizing the main geological events that occurred in the neighbouring areas of the Pangea super-continent since its formation during the Variscan Orogeny and until its early break-up phases during Late Triassic time.

2. Geological outline

2.a. Palaeogeography and geodynamics of Adria

The Southern Alps in central Europe are a structural domain delimited by the Periadriatic line to the north and west, by the Po and Venetian–Friulian plains to the south and by the Slovenian Karst plateau to the east. During late Palaeozoic – early Mesozoic time, the Southern Alps were part of the northern margin of the Adria Plate (in this work referred to as Adria, as defined by Schmid *et al.* 2008). Other units belonging or located close to Adria were Alcapa (a tectonic mega-unit including the Eastern Alps, West Carpathians and the Transdanubian ranges north of Lake Balaton; Csontos & Vörös, 2004), the external Dinarides, Apennines and the Apulian carbonate platform (Schmid *et al.* 2008). The Palaeozoic and Mesozoic geodynamics and palaeogeography of Adria and its constituent units are still being debated. Here we summarize the main aspects that are relevant to the discussion on Triassic magmatism in the Southern Alps and the possible fingerprints of its geochemistry.

According to von Raumer (1998), during late Precambrian – early Palaeozoic time, the basement units of the Alps were part of a volcanic arc at the northern margin of Gondwana. After a stage dominated by rifting during Cambrian–Ordovician to Silurian

time, the Gondwana–Laurasia collision produced a large orogenic belt that ranged from the Caucasus to the east, to the southern Appalachians and Ouachitas in North America to the west. The result of this collision in western Europe, which had its peak at the end of the Carboniferous period, is the Variscan Belt. The fingerprints of this event in the lithosphere of Adria, such as metamorphism and crustal melting, are still preserved today in the Austroalpine and South Alpine units (von Raumer, 1998). In the Southern Alps, they are also evident in the lower crustal portion of the Ivrea–Verbano exposed crustal section (Handy *et al.* 1999).

During the Permian period, the suture zone between Gondwana and Laurasia reactivated as a large right-lateral E–W-aligned shear zone (intra-Pangea dextral shear; IPDS; Muttoni *et al.* 2009) involving the eastern coast of North America, the northern part of South America, northwestern Africa and the northern margin of Adria. In the same period, an extensional system developed from Siberia to western Europe, propagating southwards and superimposing the IPDS (Nikishin *et al.* 2002). Associated with this system, significant magmatic activity occurred at the margin between Gondwana and Laurasia (e.g. Lago *et al.* 2004). At the northern margins of Adria, this activity is recorded by the Sesia magmatic system in the Ivrea–Verbano crustal section (Quick *et al.* 2009) and by volcanics and granitoid intrusions in the western and central Southern Alps (e.g. Rottura *et al.* 1998; Schaltegger & Brack, 2007; Cassinis *et al.* 2008; Bellieni *et al.* 2010), but no evidence of Permian magmatism is preserved in the Carnic and Julian Alps (Fig. 1). Contemporarily with the transtensional and extensional tectonics in western Europe, the Palaeotethys ocean subducted more to the east beneath the Euroasiatic margin (e.g. Stampfli *et al.* 2002; Muttoni *et al.* 2009).

The transtensional and extensional events in western Europe and the subduction of Palaeotethys on the east continued during the Triassic period, but the precise palaeogeographic position of Adria in this geodynamic framework is still being debated (Fig. 2). On the regional scale, the northern part of Adria was affected by Triassic extensional and strike-slip tectonics, with the formation of multiple carbonate platforms and basins

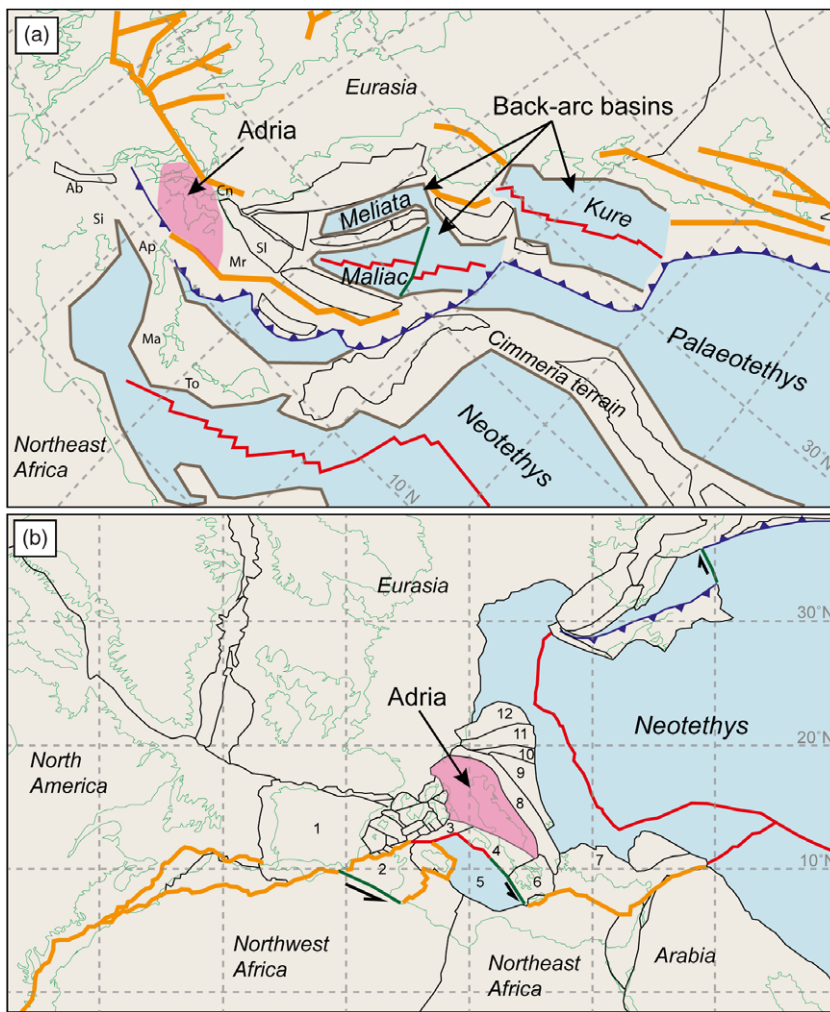


Fig. 2. (Colour online) Palaeogeography of Adria and western Tethys at 230 Ma based on (a) Stampfli (2005) and (b) Schettino & Turco (2011). Coloured lines are present-day coastlines (light green), unit boundaries (black), rifts (orange), spreading ridges (red), subduction zones (blue), passive margins (brown, shown only by Stampfli, 2005) and transform faults (dark green). Unit names in (a): Ab – Alboran; Ap – Apulia; Cn – Carnic-Julian; Ma – Mani; Mr – Mrzlevodice fore-arc; Si – Sicanian; Sl – Slavonia; To – Talea Ori. Unit names in (b): 1 – Iberia; 2 – Tunisia; 3 – Panormide platform; 4 – Apulia; 5 – Ionian Basin; 6 – southern Greece; 7 – Menderes-Taurides platform; 8 – Eastern Dinaride platform; 9 – Eastern Dinaride accretionary wedge; 10 – southern Pannonian Basin; 11 – Tisza; 12 – Pelso. Projection and rotation of the maps have been kept as per the originals (Stampfli, 2005; Schettino & Turco, 2011).

(e.g. Doglioni, 1987; Vai, 1991; Gianolla *et al.* 1998; Bortolotti & Principi, 2005; Beltrando *et al.* 2015). In this context, intense magmatic activity took place during the Triassic period in an area that today ranges from Alpine Corsica, the Southern Alps, Alcapa and Dinarides (e.g. Pamić, 1984; Castellarin *et al.* 1988; Visonà & Zanferrari, 2000; Beccaluva *et al.* 2005). Geochemical studies show that many of the Triassic magmatic rocks show an orogenic affinity and, as mentioned in the introduction, the geodynamic framework in which they originated is still being debated. Since there is no evidence of a magmatic arc (i.e. crustal metamorphism, ophiolites, predominant compressional tectonics) affecting the Adria Plate during the Triassic period, two possible geodynamic settings in which this magmatism took place have been suggested in recent years: a back-arc setting and aborted rifting associated with the opening of the Alpine Tethys.

2.a.1. Back-arc setting

Ziegler & Stampfli (2001), Stampfli *et al.* (2002), Csontos & Vörös (2004) and Golonka *et al.* (2004) suggested that, during the Triassic period, the western end of the subduction of the Palaeotethys was located just SW of Adria (Fig. 2a). Based on their model, Adria had been separated from Gondwana since the Permian period. The subduction rollback created several oceanic ridges, generally considered to be aligned in a NW–SE direction, that is, Meliata, Maliac and Pindos (Stampfli *et al.* 2002) or Vardar

and Pindos (Csontos & Vörös, 2004). According to these authors, the Triassic extensional tectonics in the Southern Alps would be related to the opening of either the Meliata or Vardar back-arc basins. Armienti *et al.* (2003) and Zanetti *et al.* (2013) suggest a similar scenario as a possible setting for the magmatic episode that affected the northern margin of Adria. Another model comes from Doglioni & Carminati (2008), who suggested a possible W-wards subduction during late Permian or Early Triassic time. This subduction might have retreated towards the east (Slovenia, Hungary) to form a back-arc basin, which might have been the trigger for the Carnian magmatism in the Southern Alps. The relic of this system is suggested now to be below the Pannonian Basin (Doglioni & Carminati, 2008).

2.a.2. Aborted rifting associated with the opening of the Alpine Tethys

A second group of authors (Bortolotti & Principi, 2005; Schmid *et al.* 2008; Muttoni *et al.* 2009; Schettino & Turco, 2011) suggested that the Adria Plate was far from the western end of the subduction of the Palaeotethys (e.g. Fig. 2b) and that the only active geodynamics around the Adria Plate during the Triassic period was extensional or transtensional. In their reconstructed palaeogeography, Bortolotti & Principi (2005) and Schmid *et al.* (2008) suggested that the northern passive margin of Adria faced the western sector of the Neotethys, while Schettino & Turco (2011) show that

the Dinaric and Pannonian units separated Adria from this oceanic realm (Fig. 2b). Bortolotti & Principi (2005) and Schettino & Turco (2011) suggested that the extensional and/or transtensional tectonics were associated with the early rifting stages of the Alpine Tethys, which opened later in the Jurassic period. Schettino & Turco (2011) provided the most detailed scenario, in which rifting began during Late Triassic and Early Jurassic times at the western, northern and eastern margins of the Adria Plate, but culminated with an oceanic spreading centre only at the western margin. The geodynamic models for the origin of Triassic magmatism suggested by Sloman (1989), Beccaluva *et al.* (2005) and Beltràn-Triviño *et al.* (2016) are consistent with this scenario.

2.b. Triassic magmatism in the Southern Alps and western Alcapa

Triassic igneous and volcanoclastic rocks crop out at several localities over the entire area of the Southern Alps and in some areas of the northeastern Alps (Fig. 1). In the westernmost Southern Alps, magmatic products are mainly represented by some lithologies of the Finero complex, Ivrea–Verbano zone (e.g. Siena & Coltorti, 1989; Zanetti *et al.* 2013). The Finero complex is an exposed section of lower continental crust composed of phlogopite-bearing peridotites at the core, surrounded by a layered pluton referred to as the 'Finero mafic complex' by Zanetti *et al.* (2013). Zircon U–Pb ages and Sm–Nd isochron ages record an intricate thermal and magmatic history for this complex, spanning Permian–Jurassic time (e.g. Lu *et al.* 1997a; Stähle *et al.* 2001; Zanetti *et al.* 2013; Langone *et al.* 2017). However, at least part of this complex records a Late Triassic intrusion age (232 ± 3 Ma; Zanetti *et al.* 2013) and several alkaline pegmatitic dykes show U–Pb zircon ages in the range 239–208 Ma (see review in Zanetti *et al.* 2013).

In the area between Lake Maggiore and Lake Garda, Triassic magmatism mainly crops out as pyroclastic products, lava flows and subvolcanic rocks, which are interbedded with carbonate sequences and continental terrigenous or transitional deposits of Anisian – early Carnian age (e.g. Crisci *et al.* 1984; Cassinis *et al.* 2008; Beltràn-Triviño *et al.* 2016). Zircon U–Pb ages of the pyroclastic layers, which also crop out north of the Periadriatic Line (Furrer *et al.* 2008), show a peak activity at *c.* 245–235 Ma (Beltràn-Triviño *et al.* 2016; Storck *et al.* 2019). Age data for the lava flows and minor associated sills and dykes cropping out north of Brescia (Fig. 1) are limited to two Rb–Sr ages (231 ± 5 and 226 ± 4 Ma) for two dacitic rocks with calc-alkaline affinity (Cassinis & Zezza, 1982; Cassinis *et al.* 2008) and to one Ar/Ar age for a basaltic dyke with tholeiitic affinity (217 ± 3 Ma; Cassinis *et al.* 2008). Just east of Lake Garda in the area of Recoaro (north of Verona; Fig. 1) there are rhyolites to dacites and minor basaltic lava flows and small intrusives with shoshonitic affinity (De Vecchi & Sedeà, 1983; Bellieni *et al.* 2010; Lustrino *et al.* 2019). They lie on the pelagic units of the Nodosus Formation, which have been assigned a late Ladinian age by De Vecchi & Sedeà (1983). No published isotopic age data are available for these outcrops.

Further east, the area of the Dolomites includes well-exposed intermediate to acid intrusions (Mount Monzoni and Predazzo intrusive complexes), pyroclastic layers, basaltic lava flows, numerous basaltic dykes and sills with shoshonitic affinity, and lamprophyric dykes, often including mantle xenoliths (e.g. Sloman, 1989; Gasparotto & Simboli, 1991; Bonadiman *et al.* 1994; Visonà, 1997; Carraro & Visonà, 2003; Casetta *et al.* 2018a, b, 2019; Lustrino *et al.* 2019; Storck *et al.* 2019). In the Dolomites, Triassic sills and lava

flows lie between the Livinnallongo and Conglomerato della Marmolada formations (of Ladinian age, according to Gasparotto & Simboli, 1991). Rb–Sr and $^{40}\text{Ar}/^{39}\text{Ar}$ dating of the intrusives and subvolcanic rocks of the Mount Monzoni and Predazzo volcano-plutonic complexes yields ages of 238–230 Ma (Borsi & Ferrara, 1968; Laurenzi *et al.* 1994; Laurenzi & Visonà, 1996), with the exception of the lamprophyres from Predazzo (219.22 ± 0.73 Ma; Casetta *et al.* 2019). Zircon U–Pb geochronology on a few intermediate to acid intrusives from the same complexes and on volcanic ash beds from the Western Dolomites suggest an interval between 242.65 ± 0.04 and 237.58 ± 0.04 Ma (Storck *et al.* 2019).

In the Carnic and Julian Alps (eastern Southern Alps), the only basic products are the lava flows from Forni di Sopra (Carnic Alps), which stratigraphically appear slightly younger and lie inside the Livinnallongo Formation (Carnian). In this area, intermediate to acid tuff layers, volcanoclastic deposits and ignimbrites are more abundant. The most representative are the Rio Freddo volcanic rocks, which lie between the limestones of the Calcari di Pontebba and the Dolomia dello Sciliar formations; these are attributed to the late Anisian and Ladinian ages by Gianolla (1992), respectively. Isotopic age data for these units are missing.

On the easternmost side, Triassic magmatism is represented by the northern part of the Karawanken plutonic belt (Austria; Visonà & Zanferrari, 2000; Bole *et al.* 2001; Miller *et al.* 2011), which crop out just north of the Periadriatic Line, in the Alcapa mega-unit. It is composed by alkaline gabbros, monzonites, syenites and syenogranites. Available ages range from 221 ± 6 Ma (whole rock Rb–Sr isochron; Visonà & Zanferrari, 2000) to 238 ± 2 Ma (mineral-whole rock Sm/Nd isochron; Miller *et al.* 2011).

3. Sampling

A total of 146 samples of lava flows, sills, dykes, plutonic rocks and ignimbrites were collected in the eastern sector of the Southern Alps, from the Dolomites to the Julian Alps (Fig. 1). Where possible, lava flows were preferentially sampled in order to minimize the effect of contamination from the carbonate country rocks, which is common in the intrusive and sub-intrusive Triassic rocks of the Dolomites. Sampling locations are shown in Figure 3. Samples from the Western Dolomites include lava flows, dykes and minor sills and intrusives. Among the dykes, we also sampled a lamprophyric dyke from Predazzo cutting Triassic volcanics of Mount Mulat. In the Eastern Dolomites, sills were mainly sampled with only a few lava flows and dykes, including another lamprophyre. In the Carnic Alps a few lava flows cropping out close to the village of Forni di Sotto were collected, and in the Julian Alps some samples of ignimbrites from the Rio Freddo volcanic rocks were collected close to the town of Tarvisio.

4. Analytical methods

Mineral compositions were determined by a Cameca SX50 electron microprobe at the Institute for the Geosciences and Georesources, Consiglio Nazionale delle Ricerche (CNR), Padova, Italy. Operating conditions of the instrument were: 15 kV acceleration voltage, 15 nA beam current, counting times of 10 s for peak and 10 s for background (i.e. 5 s for each side of the peak), and *c.* 2 μm spot size. Natural and synthetic minerals were used as standards. X-ray counts were converted into weight per cent oxides using Cameca PAP software.

Whole-rock major elements for the majority of the samples were performed using a X-ray fluorescence (XRF) spectrometer

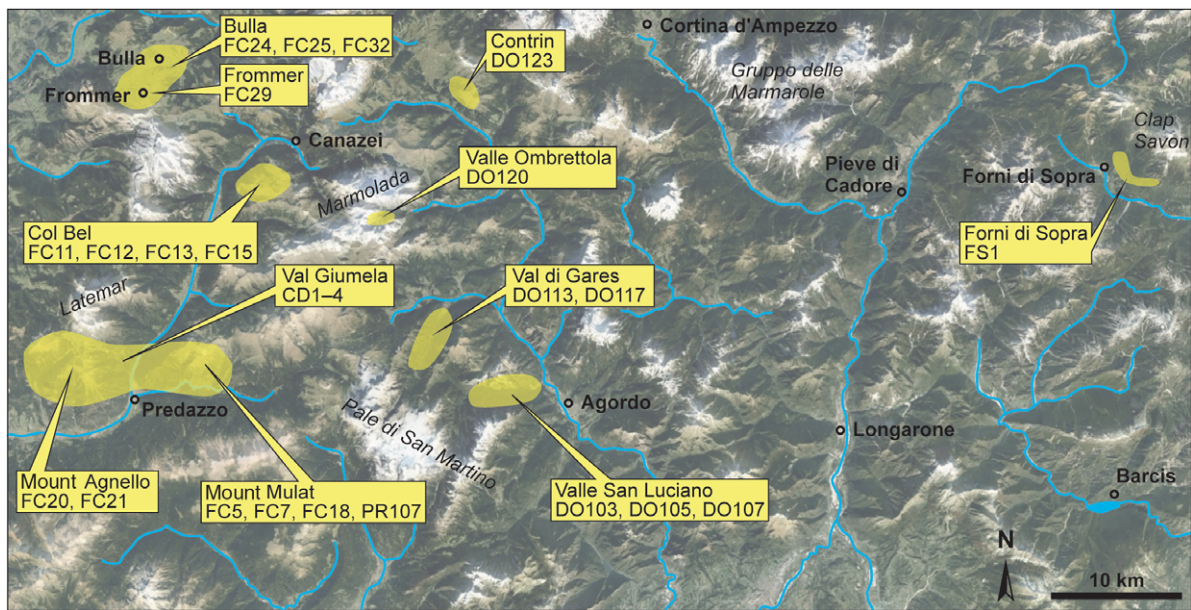


Fig. 3. (Colour online) Sampling locations (yellow areas) in the Dolomites (west) and Carnic Alps (east). The list of selected samples (yellow squares) for each locality is also reported. Background map is from Google Earth Pro®, version 7.3.2.5776, imagery date 10/23/2019, eye altitude 73 km.

Philips 1404 at the Department of Mathematics and Geosciences, University of Trieste, after preparing pressed powder pellets. The resulting errors were less than 2%. Analysis of the remaining samples (CD1, CD2, CD3 and CD4) was carried out on glass beads with a XRF spectrometer WDS Philips PW2400 at the Department of Geosciences, University of Padova. The Cross, Irving, Pirsson and Washington (CIPW) data (Cross *et al.* 1902) and the Mg number (Mg no. = $\text{Mg}/[\text{Mg}+\text{Fe}^{2+}]$) were calculated assuming a $\text{Fe}_2\text{O}_3/\text{FeO}$ ratio of 0.20, here assumed to be an average value for alkaline magmas (e.g. Moussalam *et al.* 2014; Grocke *et al.* 2016).

Trace elements were analysed using the inductively coupled plasma – mass spectrometry (ICP-MS) at ACME Labs (Vancouver, Canada) and at the Centre de Recherches Pétrographiques et Géochimiques (CRPG) Centre national de la recherche scientifique (CNRS) laboratory at Vandoeuvre les-Nancy (France). Since the loss of ignition (LOI) values are rather high in most of the collected samples, because of the presence of vacuoles filled by secondary carbonates, we performed a leaching for all the selected samples via a 0.1 mol solution of HCl at room temperature for 1 minute before analysing isotope ratio. Isotopic analyses were performed at the Department of Mathematics and Geosciences, University of Trieste and at the Department of Earth Sciences, University of Geneva, Switzerland. In Trieste we measured the isotope ratio of Sr ($^{87}\text{Sr}/^{86}\text{Sr}$) and Nd ($^{143}\text{Nd}/^{144}\text{Nd}$) using a VG Isomass 54E mass spectrometer, following Doroozi *et al.* (2016). The isotopic fractionation was corrected using the value $^{88}\text{Sr}/^{86}\text{Sr} = 0.1194$. The standards NBS987 and JNd1 yielded a mean value of 0.71025 ± 2 ($n = 20$) and 0.51210 ± 2 ($n = 5$), respectively.

In Geneva, we measured the isotope ratios of Sr ($^{87}\text{Sr}/^{86}\text{Sr}$), Nd ($^{143}\text{Nd}/^{144}\text{Nd}$) and Pb ($^{206}\text{Pb}/^{204}\text{Pb}$, $^{207}\text{Pb}/^{204}\text{Pb}$, $^{208}\text{Pb}/^{204}\text{Pb}$) using a Thermo Neptune Plus Multi-Collector ICP-MS in static mode. The method is described in detail in Chiaradia *et al.* (2011) and Beguelin *et al.* (2015). Between 100 and 120 mg of whole-rock powder were dissolved over 7 days in Savillex® Teflon vials using 4 mL of concentrated HF and 1 mL of 14 M HNO_3 at a temperature of 140°C, and with the help of ultrasonication for 30 minutes twice a day. Subsequently, samples were dried and redissolved for 3 days

(also with 30 minutes ultrasonication twice a day) in 3 mL of 14 M HNO_3 and dried again. Sr, Nd and Pb were then separated using cascade columns with Sr-Spec, Tru-Spec and Ln-Spec resins according to a protocol modified from Pin *et al.* (1994). Finally, the material was redissolved in 2% HNO_3 solutions and ratios were measured using a Thermo Neptune Plus Multi-Collector ICP-MS in static mode. Ratios used to monitor internal fractionation were: $^{88}\text{Sr}/^{86}\text{Sr} = 8.375209$ for the $^{87}\text{Sr}/^{86}\text{Sr}$ ratio, $^{146}\text{Nd}/^{144}\text{Nd} = 0.7219$ for the $^{143}\text{Nd}/^{144}\text{Nd}$ ratio and $^{203}\text{Tl}/^{205}\text{Tl} = 0.418922$ for the three Pb ratios (a Tl standard was added to the solution). Used external standards were SRM987 ($^{87}\text{Sr}/^{86}\text{Sr} = 0.710248$, long-term external reproducibility: 10 ppm), JNd1-1 ($^{143}\text{Nd}/^{144}\text{Nd} = 0.512115$; Tanaka *et al.* 2000; long-term external reproducibility: 10 ppm), and SRM981 (Baker *et al.* 2004) for Pb (long-term external reproducibility of 0.0048% for $^{206}\text{Pb}/^{204}\text{Pb}$, 0.0049% for $^{207}\text{Pb}/^{204}\text{Pb}$ and 0.0062% for $^{208}\text{Pb}/^{204}\text{Pb}$). $^{87}\text{Sr}/^{86}\text{Sr}$, $^{143}\text{Nd}/^{144}\text{Nd}$ and Pb isotope ratios were further corrected for machine bias (as a result of a systematic difference between measured and accepted standard ratios) by values of -0.039‰ , $+0.047\text{‰}$ and $+0.5\text{‰}$ amu respectively. Interferences at masses 84 (^{84}Kr), 86 (^{86}Kr) and 87 (^{87}Rb) were corrected by monitoring ^{83}Kr and ^{85}Rb ; ^{144}Sm interference on ^{144}Nd was monitored on the mass ^{147}Sm and corrected using a $^{144}\text{Sm}/^{147}\text{Sm}$ value of 0.206700; and ^{204}Hg interference on ^{204}Pb was corrected by monitoring ^{202}Hg . Total procedural blanks were <500 pg for Pb and <100 pg for Sr and Nd, which are insignificant compared with the amounts of these elements purified from the whole-rock samples investigated.

5. Sample selection and classification

Of the 146 samples, a first careful screening based on the observation of hand specimens and thin-sections resulted in the exclusion of 70 samples as they showed high degrees of hydrothermal alteration. The remaining 76 samples were selected for whole-rock major- and trace-element chemical analysis (XRF). Further selection of the less-altered samples was also performed by considering rock type and sampling location, leaving 26 representative samples

Table 1. Description of the selected samples and analytical methods of investigation

Sample	Area	Locality	Type	Classification	WR XRF	WR ICP-MS	Sr isotopes	Nd isotopes	Pb isotopes	EPMA
Basaltic suite										
FC5	WD	Mt. Mulat	LF	BTA		VA	TS	TS		PD
FC7	WD	Mt. Mulat	LF	TAN		TS				
FC11	WD	Col Bel	LF	TRB		VA				PD
FC12	WD	Col Bel	LF	BAA		TS				
FC13	WD	Col Bel	LF	BAA		NA	GE	GE	GE	
FC15	WD	Col Bel	LF	BTA		TS				
FC18	WD	Mount Mulat	LF	MZ		VA	GE	GE	GE	
FC20	WD	Mount Agnello	LF	MZ		TS				
FC21	WD	Mount Agnello	LF	BTA		TS				
FC24	WD	Bulla	LF	BTA		NA				
FC25	WD	Bulla	LF	TRB		TS				
FC29	WD	Frommer	LF	TRB		NA	GE	GE	GE	
FC32	WD	Bulla	LF	BTA		TS				
CD1	WD	Val Giumela	LF	BAS		PD				PD
CD2	WD	Val Giumela	LF	BAS		PD				PD
CD3	WD	Val Giumela	LF	TRB		PD				PD
CD4	WD	Val Giumela	LF	BTA		PD				PD
DO103	ED	Valle San Luciano	Sill	G		VA	GE	GE	GE	PD
DO105	ED	Valle San Luciano	Sill	BTA		TS				
DO107	ED	Valle San Luciano	Sill	BAA		TS				
DO113	ED	Val di Garès	Sill	BAA		TS				
DO117	ED	Val di Garès	Sill	BAS		NA	TS	TS		PD
DO120	ED	Valle Ombrettola	Dyke	BTA		VA	GE	GE	GE	PD
FS1	CA	Forni di Sopra	LF	BTA		VA	TS	TS		PD
Lamprophyres										
DO123	ED	Contrin	Dyke	TEP		VA	TS	TS		PD
PR107 ^a	WD	Mount Mulat	Dyke	BAS		VA	GE	GE	GE	PD

CA – Carnic Alps; BAA – basaltic andesite; BAS – basalt; BTA – basaltic trachyandesite; ED – Eastern Dolomites; G – gabbro; LF – lava flow; MZ – monzogabbro; TAN – trachyandesite; TEP – tephrite; TRB – trachybasalt; WD – Western Dolomites. Analyses performed at the University of Trieste (TS), University of Padua (PD), ACME Labs, Vancouver (VA), CRPG-CNRS Laboratory at Vandoeuvre les-Nancy (NA) and University of Geneva (GE).

^aMajor- and trace-element and isotopic analyses performed separately on the matrix and the amphibole megacrysts

(Table 1) investigated in detail for petrography, mineral chemistry and trace elements. Among these, 10 samples were further analysed to obtain Sr and Nd isotopic ratios, of which 6 were also investigated for Pb isotopes (Table 1). The sampling sites for these selected rocks are shown in Figure 3.

Figure 4 shows the composition of all 76 analysed samples plotted in the total alkali silica (TAS) classification diagram of Le Bas *et al.* (1992). The large scatter of the entire sample suite may be at least partially related to hydrothermal alteration, which causes a shift to higher Na and K contents of the rocks as a result of the presence of zeolites, or an increase of the silica content as a result of the replacement of the glass matrix by hydrothermal silica. If only the 26 selected samples are considered, the general spread of compositions is reduced and the selected rocks fall within the central part (Basalt to basaltic trachyandesite fields) of the TAS diagram, with the exception of the two lamprophyres. Since the TAS diagram does not discriminate possible transitional rock types, we

additionally used the alkaline–subalkaline subdivision of Miyashiro (1978; Fig. 4) and the R1–R2 diagram of de la Roche *et al.* (1980; online Supplementary Fig. S1). According to these classification schemes, the studied rocks display a transitional character between alkaline and tholeiitic. This is also supported by the calculated CIPW normative compositions, which yield mostly normative hypersthene and olivine and lack nepheline and quartz. Exceptions are samples FC13 and FS1, which show quartz normative of 5% and 2%, respectively (Table 2).

Based on the above classification schemes, textural and mineralogical features and locations, we subdivided the samples into three main groups.

Basaltic suite. This group identifies the selected samples that are either basalts or compositions consistent with a liquid line of descent starting from a basaltic primary magma. In the TAS diagram (Fig. 4), they classify as basalts, basaltic andesites, trachybasalts, basaltic trachyandesites and trachyandesites. Due to their

Table 2. Major and minor elements (wt%; normalized to 100 wt% anhydrous) and some relevant CIPW normative minerals of some representative samples of the basaltic suite and lamprophyres. LOI – loss on ignition

Sample	FC5	FC13	FC18	FC29	DO103	DO117	DO120	FS1	PR107GR	DO123
SiO ₂	53.32	54.21	53.43	49.51	47.58	50.09	51.13	54.71	45.54 ^a	47.21
TiO ₂	0.79	0.96	0.84	0.87	1.09	1.03	0.92	1.21	1.83	1.96
Al ₂ O ₃	16.12	17.28	15.79	15.01	11.22	16.64	18.33	19.56	18.88	18.75
Fe ₂ O ₃ ^{tot}	10.32	8.34	10.74	12.89	14.82	11.06	11.29	7.58	13.09	9.74
MnO	0.19	0.20	0.18	0.20	0.24	0.17	0.23	0.09	0.17	0.09
MgO	4.42	2.88	4.27	7.28	9.68	5.03	3.36	4.20	2.95	6.46
CaO	8.42	10.62	7.95	7.92	11.48	10.75	8.30	6.62	11.58	8.56
Na ₂ O	2.47	2.52	2.85	3.19	1.76	2.38	3.31	4.11	2.42	2.69
K ₂ O	3.60	2.59	3.55	2.77	1.87	2.47	2.64	1.65	2.63	3.91
P ₂ O ₅	0.36	0.40	0.39	0.35	0.26	0.37	0.48	0.27	0.92	0.63
LOI	0.60	4.23	1.00	4.78	1.90	2.48	2.60	3.10	–	7.70
Quartz ^b	0.31	5.02	0.00	0.00	0.00	0.00	0.00	2.01	–	0.00
Nepheline	0.00	0.00	0.00	3.15	0.58	0.00	0.00	0.00	–	7.38
Hypersthene	12.44	5.31	10.63	0.00	0.00	3.18	4.09	14.02	–	0.00
Olivine	0.00	0.00	1.23	14.71	15.66	6.28	6.14	0.00	–	11.99

^aComposition of the groundmass of lamprophyre PR107; ^bCalculated CIPW normative mineral abundance (wt%).

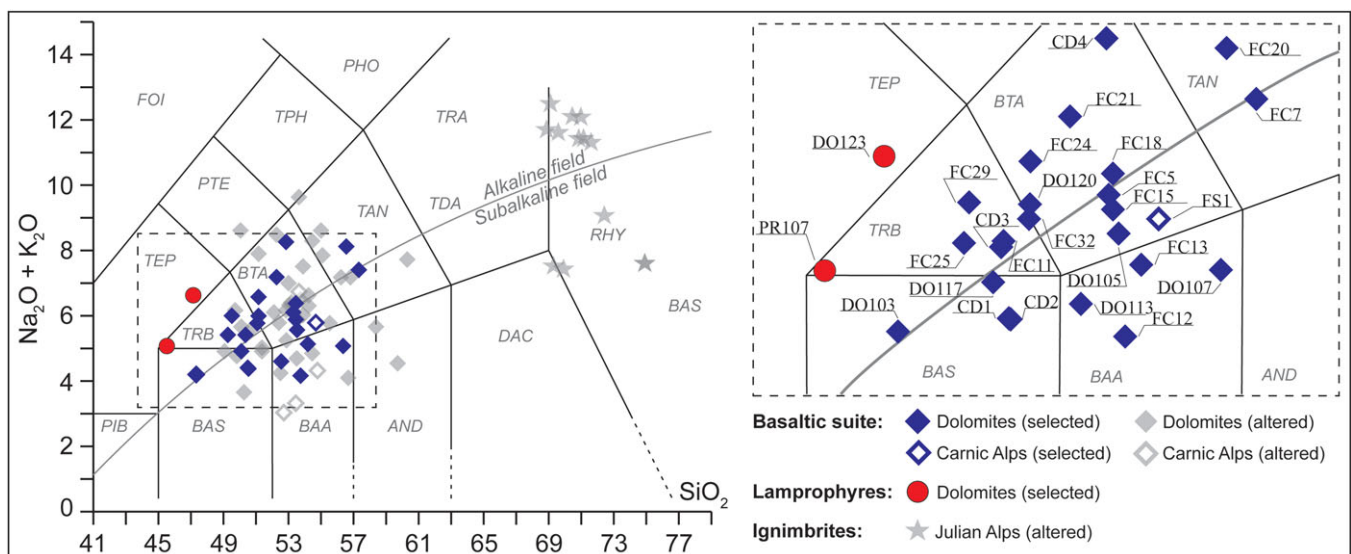


Fig. 4. (Colour online) Na₂O + K₂O v. SiO₂ wt% (TAS) classification diagram after Le Bas *et al.* (1992). Chemical data have been normalized to 100 wt% anhydrous. The grey line represents the alkaline–subalkaline boundary of Miyashiro (1978). AND – andesite; BAA – basaltic andesite; BAS – basalt; BTA – basaltic trachyandesite; DAC – dacite; FOI – foidite; PIB – picritic basalt; PHO – phonolite; PTE – phonotephrite; TPH – tephriphonolite; RHY – rhyolite; TAN – trachyandesite; TDA – trachydacite; TEP – tephrite; TRA – trachyte; TRB – trachybasalt. The intrusive samples FC18, FC20 (monzogabbros) and DO103 (gabbro) are plotted only for comparison.

chemical affinities, we also included in this group a gabbro (DO103) from Cima Pape (Agordo, Dolomites) and two monzogabbros (FC18, FC20) from Mount Mulat and Mount Agnello, Dolomites. Even although these monzogabbros appeared to be unaltered and had been collected as far as possible from a contact-metamorphic aureole cropping out in the area, they received only minimal consideration because of the likely contamination by widespread exo- and endo-skarn. This suite also includes basaltic lava flows from the Carnic Alps, which are in general more sodic and evolved. As a result of the extensive alteration, it was possible to select only one relatively unaltered sample (FS1) as representative of this locality.

Lamprophyres. These two samples (PR107 and DO123) are from the Dolomites. They were identified as lamprophyres because of their paragenesis (see Section 6.b below) and their relatively low K₂O/Na₂O (<3.0; Woolley *et al.* 1996). Following Le Maitre *et al.* (2002), and as suggested by Carraro and Visonà (2003), they belong to the camptonite family as they show the sporadic presence of clinopyroxene, the presence of altered olivine and a high modal plagioclase/K-feldspar ratio. Sample PR107 includes amphibole megacrysts that show idiomorphic shape and concentric zoning patterns, suggesting that they are phenocrysts rather than xenocrysts, in agreement with the observations of Carraro

and Visonà (2003). Due to the large size of these amphibole crystals (1–15 cm), separate chemical analyses were performed on amphibole megacrysts and on the groundmass. The whole-rock composition was calculated by mass balance, adding 20% of amphibole (its estimated modal amount) to the groundmass composition. Such a calculated composition classifies the rock as trachybasalt, that is, slightly more evolved than DO123, which classifies as tephrite.

Ignimbrites from the Julian Alps. In the TAS classification diagram, these fall within the rhyolite field. These samples are moderately and are therefore only briefly discussed. These rocks are generally the products of explosive volcanism and pyroclastic flows.

6. Petrography

6.a. Basaltic suite

Dykes and lava flows from the Dolomites generally show a medium- to fine-grained porphyritic texture, often seriated. The phenocrysts are represented by augite, strongly zoned plagioclase and olivine, which can be altered (e.g. serpentinized or reabsorbed in opaque minerals). Generally, the groundmass is glassy and altered, or microgranular. Microlites comprise the same minerals as described above, with the exception of a few more evolved samples in which sanidine can be present. The most common accessory mineral is apatite, while biotite is found in only a few samples.

The two selected monzogabbros from Mount Mulat (FC18) and Mount Agnello (FC20) show an idiomorphic texture. The major phases are slightly altered idiomorphic plagioclase, allotriomorphic K-feldspars and augite locally recrystallized as brown amphibole. Accessory phases are opaque minerals (macroscopically identified as magnetite and sulfides), apatite, biotite, rare sphene and zircon.

The San Luciano Valley gabbro (DO103), representing the inner part of a 100-m-thick sill, shows an idiomorphic texture with grain size medium to coarse. The main phase is represented by euhedral to subeuhedral clinopyroxene crystals, while plagioclase, olivine (often iddingsitized) and alkali feldspar are subordinated. The accessory phases are opaque minerals and apatite.

Secondary minerals are often present in the basaltic suite from the Dolomites. Carbonates are the main phases but zeolites, chlorites, amphiboles and products related to plagioclase alteration (e.g. albite and epidote) are also common. In some samples, small vacuoles randomly filled by carbonates, zeolites and chalcedony are present.

Lava flows from the Carnic Alps show a micro-porphyritic texture, in which the main phenocryst is plagioclase often altered to sericite, while clinopyroxene microcrystals are rare. The groundmass is hyalopilitic, with feldspathic microlites, undistinguishable pyroxenes and opaque minerals. The selected sample FS1 does not show secondary minerals, but the light-green appearance of the glassy matrix suggests slight alteration.

6.b. Lamprophyres

The lamprophyre from Mount Mulat (Predazzo; PR107) shows a coarse-grained porphyritic texture, with many idiomorphic megacrysts of zoned amphibole (1–15 cm length), rare megacrysts of plagioclase and rare phenocrysts of altered clinopyroxene. Amphibole and plagioclase also commonly appear as phenocrysts or microphenocrysts. Abundant plagioclase and rare opaque minerals are present as microlites. Accessory olivine, sometimes entirely replaced by iddingsite, is present as microlites.

The lamprophyre from Marmolada (DO123) shows a fine-grained porphyritic texture. Hornblende, more abundant than in the previous lamprophyre, is zoned. Olivine and clinopyroxenes, completely altered into saponitic products or replaced by carbonates, are abundant. Abundant plagioclase is confined to the groundmass. Secondary minerals are occasionally represented by carbonates.

6.c. Ignimbrites

The ignimbrites from the Julian Alps show an eutaxitic texture ranging from aphyric to slightly porphyroclastic. The felsic minerals (probably former plagioclase and alkali-feldspar) are often completely altered. The rare mafic minerals are completely replaced by saponitic products. Finally, the glass of the groundmass is often completely recrystallized, probably in clay minerals.

7. Mineral chemistry

Major-element compositions of olivine, pyroxenes, feldspars, amphibole and oxides are reported in online Supplementary Table S1 (available at <http://journals.cambridge.org/geo>).

7.a. Olivine

In the majority of the samples, olivine is altered, serpentinized or transformed into iddingsitic products. Fresh or partially fresh olivine crystals were only found in a few samples from the basaltic suite. From core to rim, the phenocrysts show a composition of Fo₆₈–Fo₆₄ to Fo₆₃–Fo₅₈ (Fo = mol% forsterite component). Calculated olivine/whole-rock K_D^{Fe-Mg} values are 0.29 for the lava flow CD2 and 0.52 for the dyke FC11. The latter is higher than the typical equilibrium values (0.30 ± 0.03 ; Roeder & Emslie, 1970), suggesting that olivines crystallized from melts that were more evolved than the melt composition represented by the whole-rock. The CaO content is rather high (0.29–0.41 wt%), suggesting alkaline affinity or carbonate contamination.

7.b. Pyroxenes

All the pyroxenes are classified as augites (based on Morimoto *et al.* 1988) and are characterized by TiO₂ contents generally lower than 1 wt%. Estimated Al content in the tetrahedral sites range between 0.063 and 0.240 apfu. Pyroxenes analysed in the sample FS1 (Carnic Alps) show the largest variations in TiO₂ (0.41–1.77 wt%) and Al₂O₃ (2.01–8.00 wt%). Cores and rims generally show comparable compositions with the exception of the samples from Val Giunela, for which detailed core–rim analyses were carried out (online Supplementary Fig. S2).

7.c. Plagioclase and alkali-feldspar

Plagioclase in the olivine-basalts is strongly zoned and often altered. In the fresh portions, the anorthite content (An) varies between 67–83% (core) and 62% (rim and microlites) in DO117, while in FC11 An varies between 82 and 77% without a substantial difference between core and rim/microlites.

Among the basaltic trachyandesites, plagioclase phenocrysts of sample FC5 show a clear reverse zoning with higher An at the rim (67–78%) than in the core (56–67%). This feature is in association with the presence of rare microlites of biotite in the rock. Plagioclase grains in DO120 have An contents in the range 76–87%, which suggests disequilibrium with the moderately evolved whole-rock composition (SiO₂ = 51.2 wt%; CaO/Na₂O = 2.51).

In the basaltic andesite FS1, unaltered microphenocrysts of plagioclase have a labradorite composition (An_{62-63}).

Plagioclase in the lamprophyre DO123 shows higher An in the cores (61–83%) than at the rims (38–39%). On the other hand, lamprophyre PR107 (characterized by zoned megacrysts) shows plagioclase crystals with variable An core composition spanning 38–83%, while the An at the rims ranges over 66–87%, being generally higher than within the cores. Moreover, plagioclase crystals from sample PR107 are characterized by oscillatory zoning patterns.

The few analysed sanidine crystals belong to samples DO123 (lamprophyre) and FC11 (olivine-basalt), while anorthoclase is only present in FS1 (andesitic basalt). The rare albite compositions (online Supplementary Table S1) suggest a slight spilitization related to interaction with seawater.

7.d. Amphiboles

Among the selected samples only the lamprophyres (DO123 and PR107) contain amphiboles; these are rich in Ca and show TiO_2 contents of 3.75–5.97 wt%. According to the classification scheme of Leake *et al.* (1997), the megacrysts of PR107 are mainly Fe-pargasites, few hastingsites and rare pargasites and kaersutites, while smaller crystals of DO123 are mainly kaersutites and minor pargasite. The classification diagram of Rock (1987; online Supplementary Fig. S3) shows that the analysed amphiboles fall within the alkaline-ultramafic lamprophyre field, consistent with the lamprophyric nature of these dykes. The megacrysts of PR107 plot in the region where this field overlaps with the calc-alkaline lamprophyres.

8. Whole-rock geochemistry

Whole-rock major and trace elements and Sr, Nd and Pb isotopic compositions for the selected samples are reported in Tables 2 and 3 and online Supplementary Table S2.

8.a. Major- and trace-element variations

Figure 5 shows some representative major- and trace-element data for the basaltic suite, lamprophyres and ignimbrites. Considering all the samples, a marked compositional gap separates the basaltic suite and lamprophyres ($Mg\ no. = 0.40-0.70$; $SiO_2 = 45-53\ wt\%$) from the ignimbrites ($Mg\ no. = 0.07-0.30$; $SiO_2 = 60-72\ wt\%$; Fig. 5). The basaltic suite from the Dolomites shows an increase in Al_2O_3 and an apparent decrease in FeO_{tot} with decreasing $Mg\ no.$, while all the other major elements show no clear correlations with $Mg\ no.$ With respect to samples with similar $Mg\ no.$ values, the basaltic trachyandesite FS1 from the Carnic Alps shows slightly higher SiO_2 and Al_2O_3 , and lower FeO_{tot} content compared with the Dolomitic samples. Both lamprophyres differ from the basaltic suite by showing higher contents of TiO_2 and P_2O_5 . Light rare earth element (LREE) contents show rough negative correlations with $Mg\ no.$ (e.g. Fig. 5). Variations in alkaline major elements (Na_2O and K_2O) and of large-ion lithophile elements (LILE; Rb, Ba, Sr; Table 3; online Supplementary Table S2) are likely affected by hydrothermal alteration, even for the selected samples. Regardless, Rb and K_2O , and to a lower extent Sr, display a general trend of increasing contents with decreasing $Mg\ no.$, even if the correlation is quite scattered. Nb progressively increases from the basaltic suite to the ignimbrites (6–21 ppm), but it is significantly higher in the lamprophyres (38–50 ppm).

The lamprophyres also show higher Zr and slightly higher LREE compared with the basalts.

Figure 6 shows the chondrite- (CN-) normalized REE patterns and primitive-mantle- (PM-) normalized trace-element spider diagrams for the basaltic suite and lamprophyres. Most basaltic samples from the Dolomites show similar LREE versus (v.) middle REE (MREE) and heavy REE (HREE) ratios (Fig. 6a; $La/Sm_{CN} = 2.8$; $Sm/Dy_{CN} = 2.3$; $Dy/Yb_{CN} = 1.3$; $La/Yb_{CN} = 8.2$; average values excluding DO103). The exception is the gabbro (DO103; $Mg\ no. = 0.61$), which shows slightly lower LREE contents and LREE/MREE ratios ($La/Sm_{CN} = 2.2$). FS1 (Carnic Alps) yielded slightly higher HREE concentrations ($La/Yb_{CN} = 5.6$). All the samples present a small negative Eu anomaly (average $Eu/Eu^* = 0.82$; $Eu^* = (Sm_{CN} + Gd_{CN})/2$), which may result from plagioclase fractionation. The lamprophyres (Fig. 6c) show REE patterns similar to the basaltic samples, but do not show the negative Eu anomaly ($Eu/Eu^* = 1.0-1.06$). All the REE patterns plot between those of average ocean-island basalts (OIB) (McDonough & Sun, 2005) and the upper crust as proposed by Rudnick & Gao (2003) (Fig. 6a, c). In particular, the LREE better approach the OIB composition ($La/Sm_{CN} = 2.3$), while HREE variations resemble those of the upper crustal ($Dy/Yb_{CN} = 1.7$).

In PM-normalized multi-elemental diagrams (Fig. 6b, d), the basaltic suite from the Dolomites shows marked negative Nb anomalies (v. K and La) and negative Ti anomalies (v. Hf and Y). Pb often shows positive spikes (particularly marked in samples from near the Predazzo intrusion and mineralizations) and, rarely, slightly negative anomalies. Notably, the highest Pb content is shown by sample FC5 ($Pb = 14.2\ ppm$) collected on Mount Mulat where sulphide and tungstate mineralization occurs (Bedovina mine). The mineralization is sub-contemporaneous with the Triassic magmatism, being related to the aplitic and pegmatitic products of the Predazzo granitic intrusion (Bianchi & Di Colbertaldo, 1956). Sr does not show any negative anomalies. This appears in contrast with the negative Eu anomalies observed above (both Eu and Sr easily substitute for Ca in plagioclase), and could therefore be related to the presence of very small amounts of Sr-bearing carbonate in the groundmass. Notably, in the Monzoni area the analysed Sr in carbonates reaches 1.2 wt% (R Petrini, personal communication, 2010). Compared with the basaltic suite from the Dolomites, the sample from the Carnic Alps (FS1) shows a less-accentuated Nb negative anomaly. Lamprophyres lack significant Nb and Ti anomalies and show a strong trough for Pb, which is particularly evident for the lamprophyre from Marmolada (DO123). The trace-element patterns of the basaltic suite approach the Upper Crust end-member of Rudnick & Gao (2003), in particular for Nb, LILE and Ti (Fig. 6d).

8.b. Sr, Nd and Pb isotopes

The Sr–Nd–Pb isotopic ratios of the selected representative samples are shown in Table 3 and Figures 7 and 8. The basaltic suite from the Dolomites has initial (230 Ma) Sr and Nd isotopic compositions in the range $0.70349 \pm 2 - 0.70500 \pm 1$ and $0.512240 \pm 1 - 0.512310 \pm 2$, respectively. These values are similar to those obtained for the Predazzo intrusive complex ($0.70399 \pm 7 - 0.70620 \pm 4$ and $0.51219 \pm 7 - 0.51230 \pm 2$; Casetta *et al.* 2018a), but differ partially from the intrusive samples from Mount Monzoni ($0.70449-0.70786$ and $0.51185-0.51213$; Bonadiman *et al.* 1994). The latter are systematically more depleted in $^{143}Nd/^{144}Nd$, and plot along the mantle array extension, with the exception of one sample. Among our samples, the basalt from the Carnic Alps

Table 3. Trace-element contents (ppm), isotope ratios and calculated model ages (Ma) of some representative samples from the basaltic suite and lamprophyres

Sample	FC5	FC13	FC18	FC29	DO103	DO117	DO120	FS1	PR107GR	DO123
Rb	113	43	114	48	47	57	40	39	58	64
Ba	527	490	492	561	296	410	517	452	481	574
Th	9.6	6.1	11.7	6.6	3.7	5.5	8.8	6.3	4.8	4.7
U	2.4	1.7	2.8	1.8	1.0	1.4	2.7	2.1	1.5	1.1
Nb	10.5	8.7	11.8	7.0	6.1	7.6	10.9	16.4	54.8	37.6
Pb	14.2	10.3	6.5	7.6	4.5	8.3	6.0	5.9	6.0	1.7
Sr	823	732	792	666	450	667	965	539	1013	817
Zr	152	142	142	115	103	130	159	157	275	257
Y	25	21	26	25	21	22	27	27	29	27
Cr	55	36	28	89	196	139	21	35	106	82
Ni	29	22	25	23	46	36	10	10	49	56
Hf	4.4	3.6	4.2	3.0	2.9	3.3	4.3	4.3	6.0	5.7
La	31.5	25.5	33.2	25.5	17.3	23.7	30.8	23.9	43.3	33.1
Ce	71.4	53.1	73.0	52.8	40.7	50.5	71.5	56.4	92.6	74.2
Pr	8.1	6.8	8.5	6.7	5.1	6.5	8.3	6.4	9.8	8.4
Nd	32.2	27.6	34.5	26.5	22.7	26.6	36.1	25.8	37.4	34.0
Sm	6.5	5.6	6.6	6.2	4.9	6.0	6.9	5.4	6.4	6.1
Eu	1.5	1.6	1.6	1.6	1.3	1.6	1.7	1.5	2.2	1.9
Gd	5.5	5.2	5.7	5.6	4.5	5.3	5.9	5.1	5.9	5.5
Tb	0.9	0.7	0.9	0.8	0.7	0.8	0.9	0.9	1.0	0.9
Dy	4.7	3.8	4.8	4.5	3.8	4.3	4.9	5.2	5.5	5.0
Ho	0.9	0.8	0.9	0.8	0.8	0.8	1.0	1.0	1.0	1.0
Er	2.6	2.0	2.6	2.3	2.2	2.2	2.8	2.9	2.9	2.7
Tm	0.4	0.3	0.4	0.3	0.3	0.3	0.4	0.5	0.4	0.4
Yb	2.4	2.0	2.5	2.4	1.9	2.0	2.5	2.9	2.7	2.6
Lu	0.4	0.3	0.4	0.4	0.3	0.3	0.4	0.4	0.4	0.4
$^{87}\text{Sr}/^{86}\text{Sr}$	0.70630	0.70491	0.70649	0.70558	0.70564	0.70430	0.70496	0.70747	0.70372	0.70487
$^{87}\text{Sr}/^{86}\text{Sr}$ (i) ^a	0.70500	0.70437	0.70516	0.70492	0.70470	0.70349	0.70459	0.70679	0.70328	0.70413
$^{143}\text{Nd}/^{144}\text{Nd}$	0.51245	0.51250	0.51242	0.51252	0.51247	0.51252	0.51242	0.51233	0.51276	0.51238
$^{143}\text{Nd}/^{144}\text{Nd}$ (i)	0.51226	0.51231	0.51224	0.51231	0.51228	0.51231	0.51225	0.51214	0.51260	0.51222
$T_{\text{DM}}(\text{Nd})$	984	908	972	1080	1022	1031	962	1217	345	955
$^{206}\text{Pb}/^{204}\text{Pb}$		18.62805	18.62086	18.81418	18.61426		18.62520		18.52061	
$^{207}\text{Pb}/^{204}\text{Pb}$		15.66680	15.67392	15.67452	15.66460		15.66950		15.64152	
$^{208}\text{Pb}/^{204}\text{Pb}$		38.86870	38.85090	39.01060	38.78483		38.81559		38.62309	

^aInitial ratio calculated for 235 Ma.

(FS1) shows the highest $^{87}\text{Sr}/^{86}\text{Sr}_i$ and the lowest $^{143}\text{Nd}/^{144}\text{Nd}_i$ (0.70679 and 0.51214, respectively) values, similar to the samples from the Monzoni intrusion (Bonadiman *et al.* 1994). All the basalts show a decoupling between the elemental and the isotopic data (compare Fig. 7a with Fig. 7b).

The lamprophyres show the lowest $^{87}\text{Sr}/^{86}\text{Sr}_i$ and the highest $^{143}\text{Nd}/^{144}\text{Nd}_i$ values (0.70326–0.70413 and 0.51268–0.51222, respectively). PR107 appears quite depleted, similar to mid-ocean-ridge basalt (MORB) compositions, while DO123 is more enriched, plotting below the bulk earth (BE) value towards the

enriched mantle I (EMI) end-member (Hart & Zindler, 1989). Notably, the isotopically depleted lamprophyre PR107 indicates an elemental enrichment in Nd v. Sm (compare Fig. 7a with Fig. 7b).

$^{206}\text{Pb}/^{204}\text{Pb}$ v. $^{207}\text{Pb}/^{204}\text{Pb}$ and v. $^{208}\text{Pb}/^{204}\text{Pb}$ isotopic ratios of all analysed samples plot above the Northern Hemisphere reference line (NHRL; Hart, 1984) and to the right of the 4.55-Ga geochron (Fig. 8). Globally, the data plot between the compositions of Variscan meta-sediments (Koppel & Schroll, 1988) and those of the enriched mantle II (EMII) component

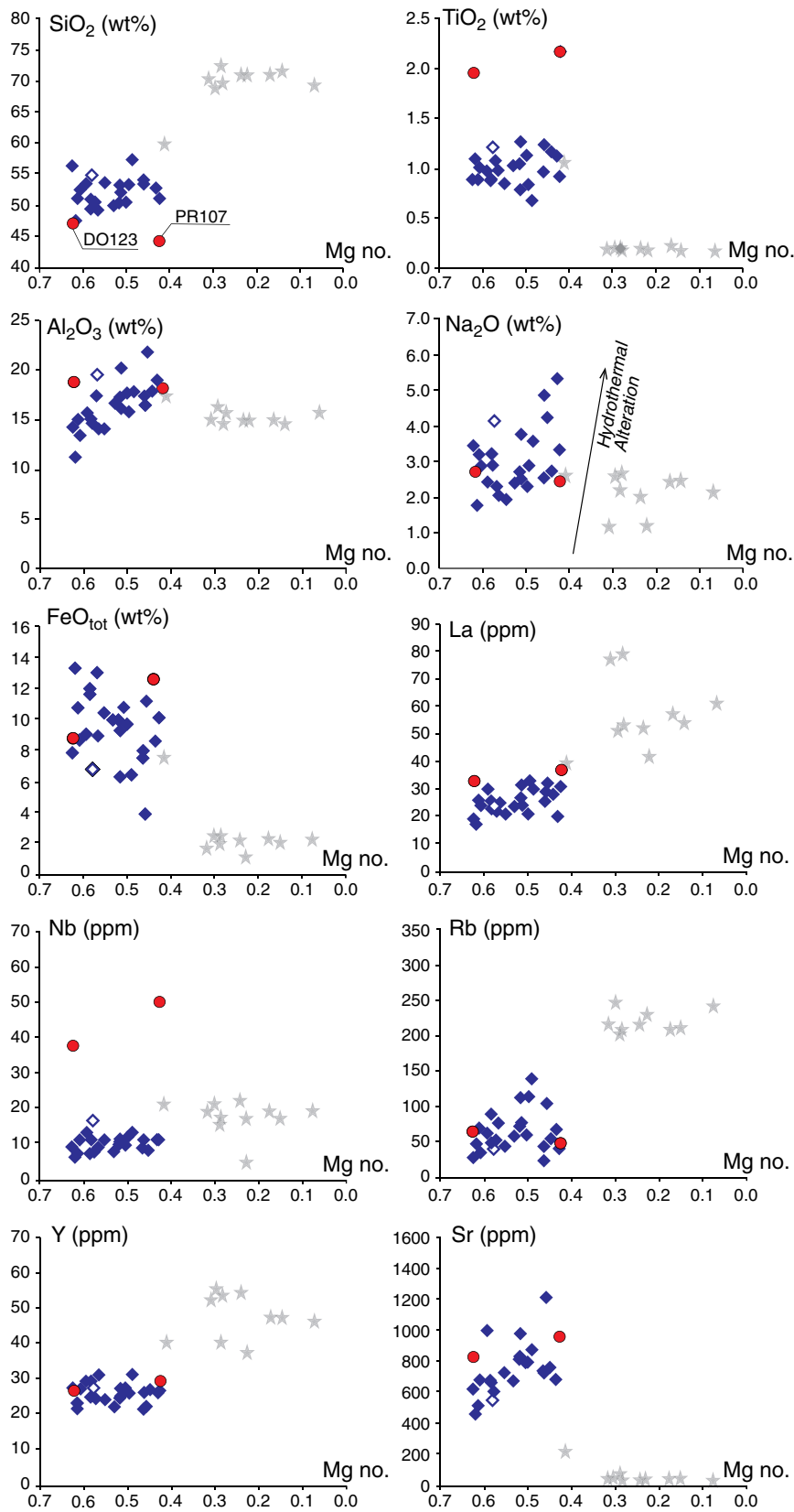


Fig. 5. (Colour online) Variations of some major (wt%) and trace elements (ppm) for the basaltic suite, lamprophyres and ignimbrites. Symbols as in Figure 4. The vector of hydrothermal alteration is an example of how Na_2O in the bulk rock would increase with increasing modal abundance of natrolite (from 0 to 35 wt%), which is a common product of hydrothermal alteration of the area.

(Hart & Zindler, 1989) and the global sea sediments (GLOSS) field (Plank & Langmuir, 1998). The lowest Pb isotopic values are shown by the lamprophyre (PR107), while the sample FC29 plots close the GLOSS field and the EMII pole. The Cu-mineralized

Bedovina rocks, interpreted as being related to the Triassic Dolomitic volcanism, plot at the low- $^{206}\text{Pb}/^{204}\text{Pb}_i$ end of our samples and overlap with the Pb isotopic compositions of the Variscan basement (Artioli *et al.* 2016).

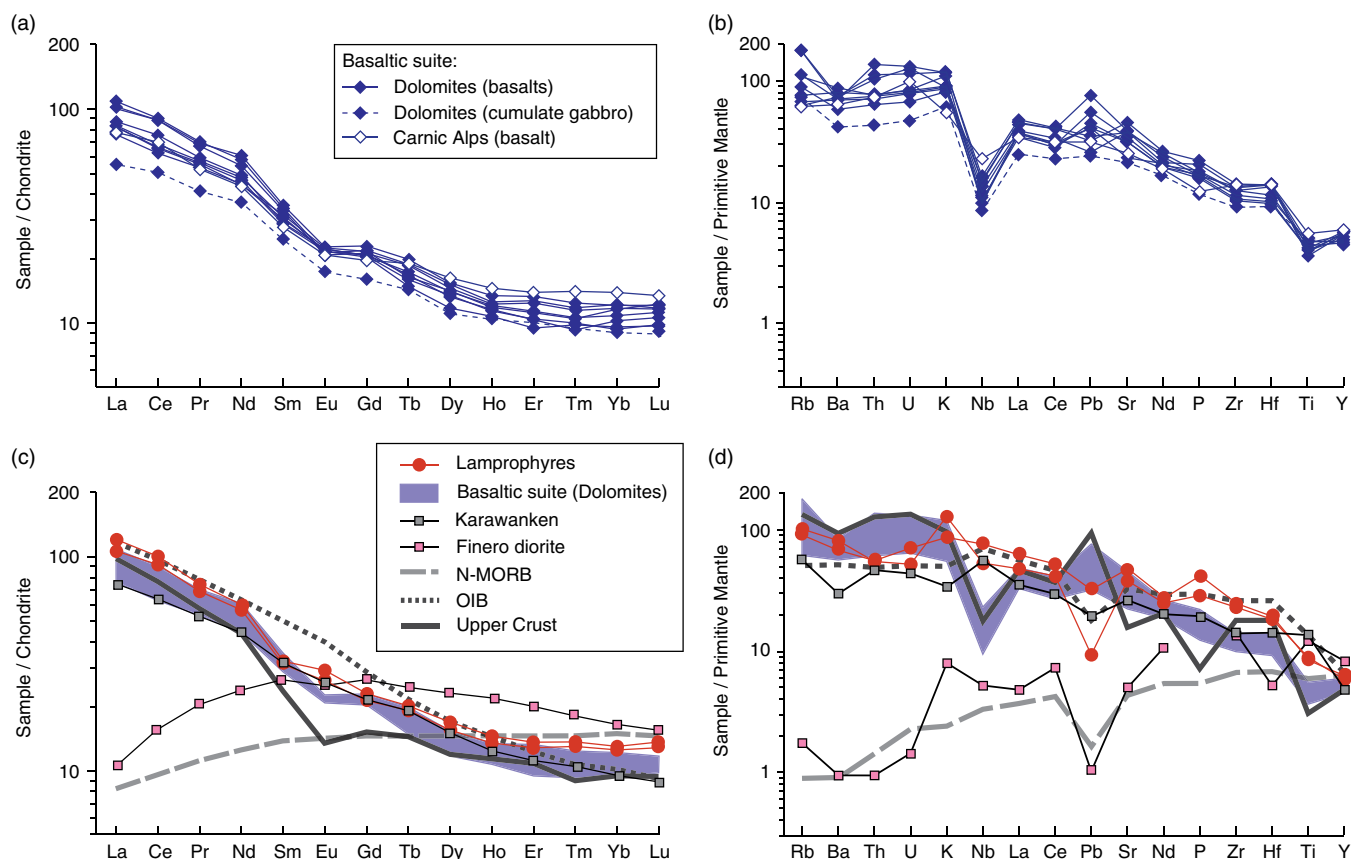


Fig. 6. (Colour online) (a, c) REE patterns (normalized to chondrites; Boynton, 1984) and (b, d) trace-element spider diagrams (normalized to primitive mantle; McDonough & Sun, 1995) for (a, b) the basaltic suite and (c, d) lamprophyres investigated in this study. (c, d) A diorite from the external gabbro unit of the Finero complex (sample F190/16; Lu *et al.* 1997b), a representative gabbro from the northern Karawanken complex (Miller *et al.* 2011) and average values of upper crust (Rudnick & Gao, 2003), OIB and N-MORB (McDonough & Sun, 1995) are shown for comparison.

8.c. Comparisons with coeval rocks from the Southern Alps and Alcapa

Trace-element contents and Sr, Nd and Pb isotopic ratios were compared with the existing data for other magmatic products attributed to Ladinian–Carnian ages in the Southern Alps and western Alcapa. In particular, we considered the basic rocks of the Karawanken complex (Visonà & Zanferrari, 2000; Miller *et al.* 2011), a Triassic diorite in the external gabbro unit of the Finero mafic complex, Italy (Fig. 1; Lu *et al.* 1997a, b), the shoshonitic magmas of the Triassic Predazzo intrusive complex (Casetta *et al.* 2018a, b) and the gabbro-monzogabbros from Mount Monzoni studied by Bonadiman *et al.* (1994).

Most of the basic Karawanken samples show REE patterns close to the basaltic samples studied in this work, while in terms of other trace elements (i.e. LILE or high-field-strength elements (HFSE) e.g. Nb) they show patterns similar to the lamprophyres. Conversely, the Finero diorite is much more depleted in trace elements and shows an REE pattern more similar to normalized- (N-) MORB magmas (Fig. 6).

The few available Sr isotopic data from the Karawanken complex ($^{87}\text{Sr}/^{86}\text{Sr}_i = 0.70313 \pm 2 - 0.70525 \pm 3$; Visonà & Zanferrari, 2000) appear quite similar to those from Dolomites, with the exception of one sample that appear less enriched (Miller *et al.* 2011; $^{87}\text{Sr}/^{86}\text{Sr}_i = 0.70496$, $^{143}\text{Nd}/^{144}\text{Nd}_i = 0.51242$). On the other hand, the Finero diorite (Lu *et al.* 1997a) differs from all the other samples, approaching an N-MORB signature and plotting close to

the lamprophyre PR107 (Fig. 7). Finally, the Mount Monzoni samples studied by Bonadiman *et al.* (1994) are moderately enriched in $^{87}\text{Sr}/^{86}\text{Sr}_i$, pointing towards EMII and overlapping the composition of the nearby Permian Cima d’Asta granite (Southern Alps; Rottura *et al.* 1998). A comparison with the recent data on Valsugana dykes from Bianchini *et al.* (2018) is reported in online Supplementary Figure S4.

In the $^{206}\text{Pb}/^{204}\text{Pb}$ v. $^{207}\text{Pb}/^{204}\text{Pb}$ and v. $^{208}\text{Pb}/^{204}\text{Pb}$ diagram (Fig. 8a, b), the Valsugana dykes (Bianchini *et al.* 2018) plot above the NHRL. With the exception of two samples, which show similar values to the Dolomitic samples of this work, the Valsugana dykes are radiogenically more enriched. Since all the Valsugana dykes show a positive Pb anomaly in the PM-normalized trace-element pattern, we suggest that the observed $^{206}\text{Pb}/^{204}\text{Pb}$, $^{207}\text{Pb}/^{204}\text{Pb}$ and $^{208}\text{Pb}/^{204}\text{Pb}$ ratios are not inherited from the source, but are probably the result of contamination by the host rocks (Variscan Metamorphic Unit).

9. Geothermobarometry and geohygrometry

A number of mineral–mineral and mineral–melt equilibria have been used to estimate the pressure (P), temperature (T) and melt H_2O contents of the magmas before eruption, using the whole-rock analyses as representative of melt compositions. A summary of the results for each individual sample is shown in Table 4 and Figure 9. For the basaltic suite, T and P were calculated iteratively using clinopyroxene–melt thermometry (Putirka, 2008, equation 33)

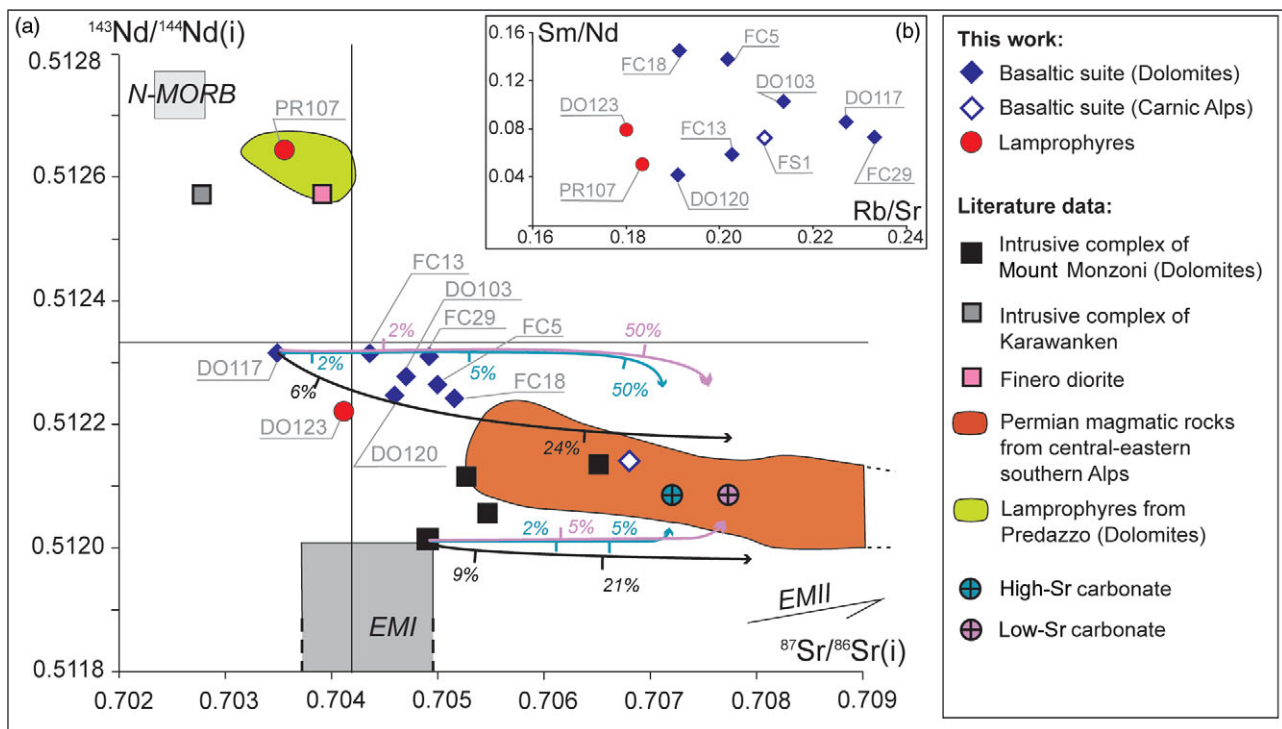


Fig. 7. (Colour online) (a) Initial (230 Ma) $^{143}\text{Nd}/^{144}\text{Nd}$ v. $^{87}\text{Sr}/^{86}\text{Sr}$ compositions of the studied samples and results of the AFC modelling using the Cima d'Asta granite (black curves) and high-Sr (blue curves) and low-Sr (pink curves) carbonates. See text for details on the modelling. The plot also includes Triassic gabbroic intrusives from Mount Monzoni (Bonadiman *et al.* 1994) and Karawanken (sample 08EK18 from Eisenkappel; Miller *et al.* 2011), lamprophyres from Predazzo (Casetta *et al.* 2019), a diorite from Finero (sample F190; Lu *et al.* 1997a) and Permian magmatic rocks (Rottura *et al.* 1998). N-MORB (light grey shaded fields), EMI and EMII were calculated for an age of 230 Ma using the isotopic values from Hart & Zindler (1989) and the elemental concentration proposed for the OIB by McDonough & Sun (1995). The bulk earth (BE) isotopic composition was recalculated at 230 Ma using elemental compositions of Sm and Nd from the recommended chondrite (Boynton, 1984) and Rb and Sr from the primitive mantle (PM) of McDonough & Sun (1995). (b) Sm/Nd v. Rb/Sr diagram.

and barometry (Neave & Putirka, 2017), assuming a melt H_2O content of 2.0 wt% (average value from hygrometric calculations, see next paragraph; we note that an error of ± 2.0 wt% in the assumed melt H_2O propagates to an error of $\pm 27^\circ\text{C}$ and 200 MPa, on average). We then used the plagioclase–melt thermometer and hygrometer of Putirka (2005, 2008) as a test for comparison.

For the basaltic suite, observed $K_D(\text{Fe-Mg})^{\text{cpx-melt}}$ for all the samples is generally within the range considered by Putirka (2008) to demonstrate equilibrium (0.27 ± 0.03), with the exception of samples DO117 (0.57) and CD1 (0.35–0.43). Average clinopyroxene–melt temperatures vary in the range 1076–1170°C, with the sample CD1 showing the higher values ($1170 \pm 14^\circ\text{C}$). Average clinopyroxene–melt pressures vary in the range 420–600 MPa, with the exception of sample FC5 with lower values (180 ± 140 MPa). Furthermore, plagioclase–melt pairs also passed the test for equilibrium [$K_D(\text{Ab-An})^{\text{plag-melt}} = 0.28 \pm 0.11$; Putirka, 2008], with the exception of sample FS1 (0.53–0.54). Plagioclase–melt and clinopyroxene–melt temperatures agree within the calculated standard deviation (Table 4). The thermodynamic model of Lange *et al.* (2009) yields average melt H_2O contents in the range 1.7–3.5 wt% for the basaltic suite from the Dolomites and a lower content for the sample from the Carnic Alps (FS1; melt $\text{H}_2\text{O} = 0.9$ wt%). The plagioclase–melt hygrometer of Putirka (2005, 2008) generally yields systematically slightly lower values (by *c.* 0.5 wt%).

Pressure and temperature was estimated for the lamprophyres using the amphibole–melt thermobarometers of Putirka (2016) and amphibole–melt thermometer and amphibole–plagioclase barometer of Molina *et al.* (2015), assuming a melt H_2O content of 6.0 wt% (in agreement with LOI values and hygrometric

calculations for the Predazzo lamprophyres studied by Casetta *et al.* 2019). Note that model errors for these methods are higher than clinopyroxene– and plagioclase–liquid methods (Table 4). Observed $K_D(\text{Fe-Mg})^{\text{amph-melt}}$ values are generally higher than that recommended by Putirka (2016) for amphibole–melt equilibrium (0.28 ± 0.11); the results of amphibole–liquid models therefore need to be considered with caution. Temperatures estimated using the amphibole–melt model of Putirka (2016) are $1046 \pm 18^\circ\text{C}$ for sample DO123 and $1003 \pm 25^\circ\text{C}$ for sample PR107, while the model of Molina *et al.* (2015) yields temperatures lower by *c.* 50°C. Application of different barometer equations (Table 4) yields values in the range 850–1250 MPa for sample DO123 and 940–1500 MPa for sample PR107.

10. Discussion

10.a. Fractional crystallization processes

The range of Mg no. (0.62–0.42), the porphyric texture and zoned crystals suggest that fractional crystallization played an important role in the genesis of the basaltic suite. However, after the careful screening to discard the most altered samples, the remaining pristine samples are few and most likely belong to different volcanic systems. A fractional crystallization modelling is therefore not applicable. Previous attempts to model the differentiation of the Triassic magmas were made by Sloman (1989), who suggested a prevalent role of clinopyroxene crystallization in the evolution of the basaltic magmas from the Western Dolomites. Accordingly, some coeval lavas from the same area host clinopyroxenite xenoliths, which are interpreted to be cumulates genetically

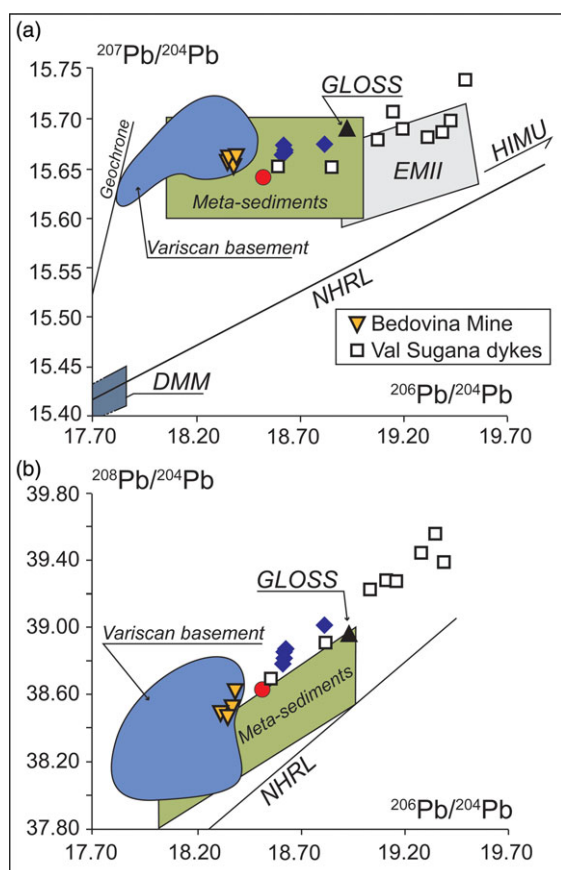


Fig. 8. (Colour online) $^{206}\text{Pb}/^{204}\text{Pb}$ v. $^{207}\text{Pb}/^{204}\text{Pb}$ and v. $^{208}\text{Pb}/^{204}\text{Pb}$ isotopic compositions of the studied rocks. The values for GLOSS (global sea sediments) are from Plank & Langmuir (1998), Val Sugana dykes from Bianchini *et al.* (2018) and Bedovina Mine samples from Artioli *et al.* (2016). The geochron, the NHRL (Northern Hemisphere reference line; Hart, 1984), and the depleted MORB mantle (DMM) and enriched mantle II (EMII; Hart & Zindler, 1989) fields are plotted for comparison. In the figure, the available compositional ranges of the Variscan crystalline basement as reported by Artioli *et al.* (2016) is plotted as representative of the Eastern Alps crustal composition. The composition of the Variscan meta-sediments as reported by Koppel & Schroll (1988) is shown for comparison. Other symbols are as in Figure 7.

related to the host magmas (Lucchini & Morten, 1977). Narduzzi *et al.* (2009) estimated the crystallization pressure for these cumulates to be c. 600 MPa, which is consistent with our estimates for the magmas based on clinopyroxene–melt barometry (400–600 MPa, with the exception of one sample). Most of the basaltic lavas, dykes and sills from the Dolomites therefore likely derived from magmas that crystallized mostly clinopyroxene at depths of c. 14–20 km. Plagioclase crystallization contributed to the evolution of the basaltic magmas, as also suggested by the CN-normalized REE patterns showing weakly negative Eu anomalies (Fig. 6a). On the other hand, the Predazzo intrusive complex is suggested to have emplaced at much shallower depths (0–7 km; Casetta *et al.* 2018a) and originated from magmas that underwent crystal fractionation dominated by plagioclase and clinopyroxene (Casetta *et al.* 2018a, b).

The low SiO_2 and high MgO contents of the lamprophyres (Table 2) suggest that they underwent only relatively minor fractional crystallization. The amphibole megacrysts in the sample PR107 suggest that amphibole was the main fractionating phase. According to the geobarometric estimates (850–1500 MPa), fractionation probably occurred close to the crust–mantle transition, which is consistent with the occasional presence of mantle xenoliths in the same family of lamprophyres from Predazzo (Carraro & Visonà, 2003).

10.b. Processes of magma–crust interaction

Sr, Nd and Pb isotopic compositions were used to put constraints on the possible interaction processes between the magmas and the Triassic and pre-Triassic crust in which they were emplaced. The possible lithologies that could have acted as contaminants were selected based on the geology of the area and the estimated storage depths of the magmas (14–20 km). Contamination could have occurred by: (1) assimilation during magma storage and differentiation in a crust possibly made by either Variscan rocks (e.g. metasediments) or refractory residues of the anatectic melting that produced the Permian acid volcanics (Rottura *et al.* 1998); or (2) post-emplacement contamination either by the Permian acid volcanics or the Permo-Triassic carbonate sediments (i.e. limestones and carbonate-bearing siltstones and marls of the Bellerophon and Werfen formations).

The $^{206}\text{Pb}/^{204}\text{Pb}$ v. $^{207}\text{Pb}/^{204}\text{Pb}$ isotopic compositions of the analysed samples overlap those of the Variscan metasediments ($^{206}\text{Pb}/^{204}\text{Pb} = 18.35\text{--}19.00$; Koppel & Schroll, 1988; Fig. 8a), while the Bedovina Mine rocks fall in the Variscan basement field as defined by Artioli *et al.* (2016), here assumed as representative of the crystalline basement of the Southern Alps. However, the Variscan metasediments have generally lower $^{208}\text{Pb}/^{204}\text{Pb}$ values than the Triassic basalts and lamprophyres, and are therefore excluded as possible contaminants.

To evaluate the possible role of the Permian acid rocks and Permo-Triassic carbonate sediments in the contamination processes of the basaltic suite, we used the assimilation-fractional crystallization (AFC) model of DePaolo (1981). The rate of assimilated/fractionated mass (r) was set to 0.3, which represents the minimum reasonable value. The distribution coefficients (D) for Sr and Nd were set to 0.8 and 0.1, respectively. Sample DO117 was used as parental composition for the Dolomitic basalts and sample CB17 (clinopyroxenite; Bonadiman *et al.* 1994) was used for the intrusive complex of Mount Monzoni. For the sample FS1 from the Carnic Alps, we assumed the same parental composition as for the Dolomitic basalts.

The isotopic composition (recalculated to 230 Ma) of the Permian granite of Cima d'Asta ($^{87}\text{Sr}/^{86}\text{Sr} = 0.71485$; $^{143}\text{Nd}/^{144}\text{Nd} = 0.51198$; $\text{Rb} = 156$ ppm, $\text{Sr} = 147$ ppm, $\text{Sm} = 3.99$ ppm, $\text{Nd} = 17.63$ ppm; Rottura *et al.* 1998) was taken as representative of the Permian acid magmatic rocks and their crustal source rocks. In this case, the AFC model suggests fractionation (F) values of 0.3 for the Dolomitic basalts, which corresponds to 9% of contamination. For the sample F2C (Basaltic dyke from Monzoni; Bonadiman *et al.* 1994) and for the FS1 basalt from the Carnic Alps F would be 0.7, which corresponds to 21% contamination. However, a fractionation of 70% is excessively high and not completely justified by the major-element composition of the magmas, which should be much more evolved. For the sample F2C this might imply important carbonate rather than silicic contamination, while for the sample FS1, this could suggest either a higher rate of assimilated/fractionated mass or an excessively low $^{87}\text{Sr}/^{86}\text{Sr}$ assumed for the contaminant. Notably, sample FS1, which crops out far from the Dolomitic area, is the only sample that shows a chemical composition consistent with important silicic contamination, being the most silica-rich sample despite a relatively high Mg no., comparable with those of the other basalts. Moreover, basaltic rocks are rare in this area (this is the only selected sample), while the acid rocks are abundant.

As representative end-member of the Permian–Triassic carbonate sediments, we used the Permian–Triassic seawater (Korte *et al.* 2003) for the Sr isotopic composition and coeval

Table 4. Temperature, pressure and melt H₂O estimates for some of the selected samples from the basaltic suite and lamprophyres

Sample	Neave & Putirka (2017); Putirka (2008)		Lange <i>et al.</i> (2009)	Putirka (2005, 2008)			Putirka (2016)		Molina <i>et al.</i> (2015)	
	Clinopyroxene–liquid		Plagioclase–liquid	Plagioclase–liquid			Amphibole–liquid		Amphibole–liquid	Amphibole–plagioclase
	<i>T</i> (°C)	<i>P</i> (MPa)	H ₂ O (wt%)	<i>T</i> (°C)	H ₂ O (wt%)	<i>T</i> (°C)	<i>P</i> (MPa)	<i>P</i> (MPa)	<i>T</i> (°C)	<i>P</i> (MPa)
	eqn 33	NP17		eqn 24a	eqn 25b	eqn 6	eqn 7a	eqn 7b		
FC11	1095 ± 11 ^a	420 ± 120	2.8 ± 0.3	1093 ± 9	2.4 ± 0.3	–	–	–	–	–
FC5	1081 ± 18	180 ± 140	1.7 ± 0.6	1101 ± 15	1.3 ± 0.5	–	–	–	–	–
CD1	1170 ± 14	580 ± 120	1.9 ± 0.4	1163 ± 14	1.1 ± 0.5	–	–	–	–	–
CD2	1103 ± 11	500 ± 110	2.9 ± 0.2	1103 ± 11	2.5 ± 0.3	–	–	–	–	–
CD3	1104 ± 9	590 ± 80	2.9 ± 0.4	1108 ± 13	2.3 ± 0.5	–	–	–	–	–
DO117	1137	600	2.0	1140	1.2	–	–	–	–	–
DO120	1077 ± 9	510 ± 140	3.5 ± 0.4	1064 ± 12	3.2 ± 0.5	–	–	–	–	–
FS1	1076 ± 13	460 ± 150	0.9	–	–	–	–	–	–	–
DO123	–	–	–	–	–	1046 ± 18	940 ± 70	850 ± 60	996 ± 7	1250 ± 100
PR107	–	–	–	–	–	1003 ± 25	150 ± 100	940 ± 50	937 ± 16	1000 ± 120
Model errors ^b	42	160	0.3	36	1.1	52	360	440	45	230

^aEach value represents the average and standard deviation of multiple analyses of the same sample, unless only one analysis is available.

^bErrors of each model as reported in the source papers. Note that standard deviations resulting from multiple analyses are well within the model errors of each method, except for the hygrometer of Lange *et al.* (2009).

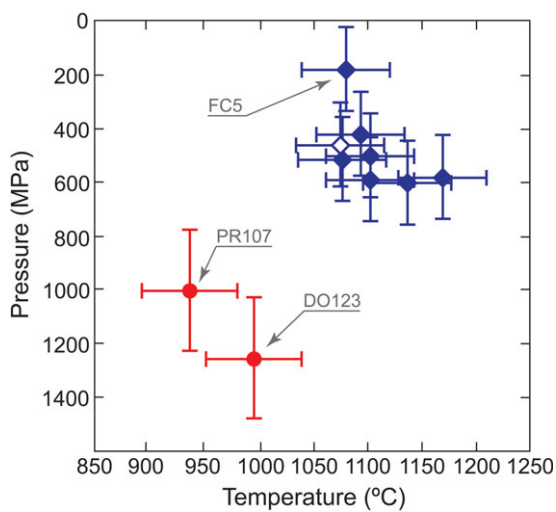


Fig. 9. (Colour online) Temperature and pressure estimates (average of multiple analyses) of the selected samples. Results for the basaltic suite refer to the clinopyroxene–melt thermometer of Putirka (2008) and clinopyroxene–melt barometer of Neave & Putirka (2017), while results for the lamprophyres refer to the amphibole–melt thermometer and amphibole–plagioclase barometer of Molina *et al.* (2015). Error bars are model errors (which are significantly higher than standard deviations of multiple analyses; see Table 4). Symbols as in Figure 4.

conodonts for the Nd isotopic ratio (Shaw & Wasserburg, 1985). We considered an Nd content of 2 ppm, calculated from the value proposed by Shaw & Wasserburg (1985). Two possible Sr contents have been used: 12 250 ppm and 2941 ppm. The first is taken from an analysed carbonate of the endo-skarn in Toal de Mason, Monzoni area, Dolomites, and the second is taken from a Triassic carbonate of the Angolo formation, Val Camonica, Lombardy (Faure *et al.* 1978). The results shown in Figure 7 highlight the effects of carbonate assimilation on the Sr isotopic

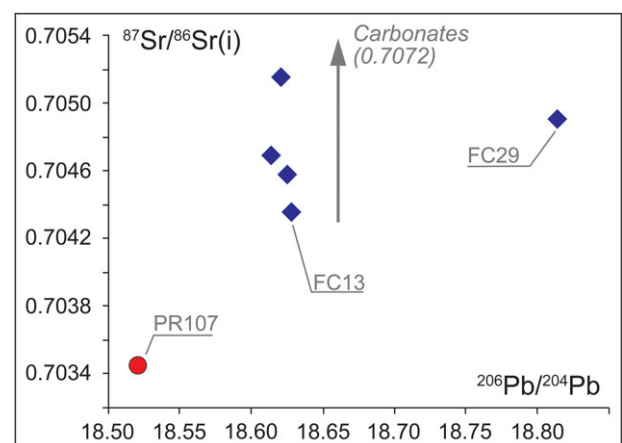


Fig. 10. (Colour online) ²⁰⁶Pb/²⁰⁴Pb with ⁸⁷Sr/⁸⁶Sr(i) diagram. The arrow shows the trend towards the ⁸⁷Sr/⁸⁶Sr values of Permian–Triassic carbonates (Korte *et al.* 2003), assuming its ²⁰⁶Pb/²⁰⁴Pb contribution is irrelevant. Symbols as in Figure 4.

composition, while Nd isotopic ratios are essentially unchanged by carbonate assimilation. The results suggest an assimilation of about 5% carbonates for the basaltic suite from the Dolomites and 10% for sample F2C of Bonadiman *et al.* (1994; Monzoni area). Such degrees of contamination should not significantly affect the major-element composition of the basaltic suite. The high ⁸⁷Sr/⁸⁶Sr_i of sample FS1 (Carnic Alps) would instead require as much as 20% of carbonate assimilation, which is an unlikely high value considering the major-element composition of this sample and its palaeogeographic position, which was far from the Triassic carbonate platforms.

The ²⁰⁶Pb/²⁰⁴Pb v. ⁸⁷Sr/⁸⁶Sr(i) diagram of Figure 10 shows two end-member compositions represented by the lamprophyre PR107 and by the basalt FC29. The basalt FC13 plots halfway between

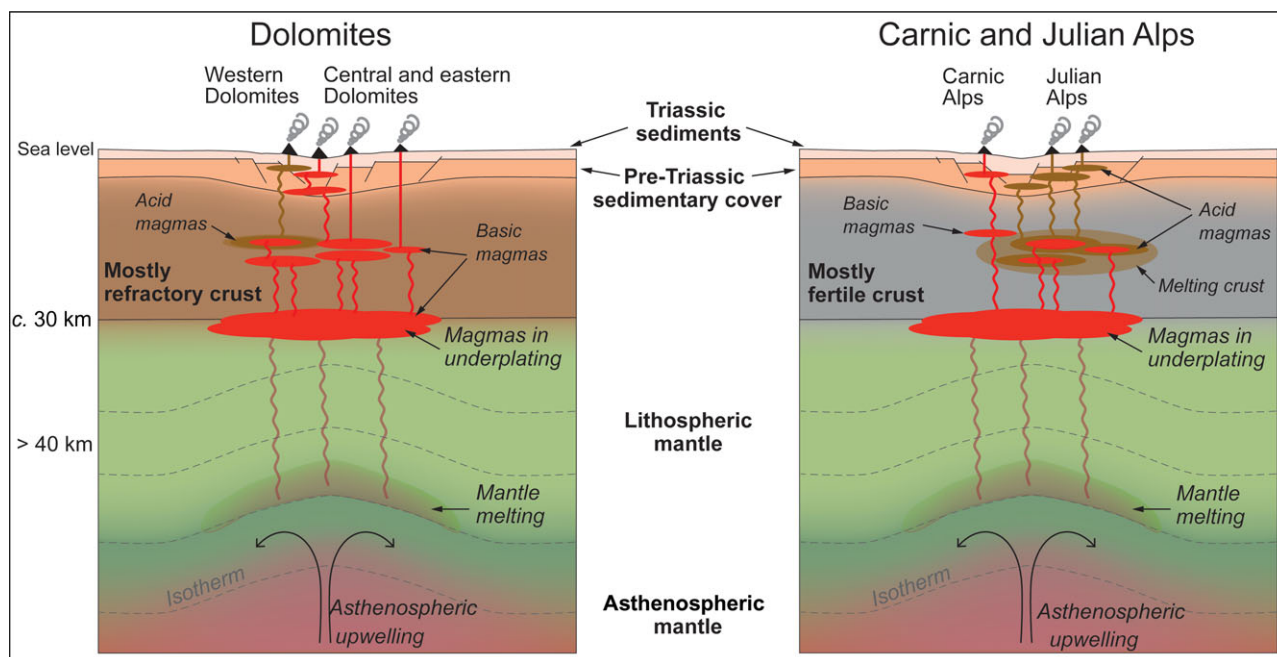


Fig. 11. (Colour online) Schematic cross-section that tentatively explains the bimodal magmatism (basaltic suite and ignimbrites) that occurred in the Dolomites and Carnic Alps (Southern Alps) during Ladinian–Carnian time. It is suggested that the crust beneath the Dolomites area was more refractory with respect to that beneath the area of Carnic and Julian Alps, which would explain the prevalent basic magmatism for the former. Depths of magmatic processes in the mantle are not well constrained; the vertical scale therefore shows only the inferred values.

these two composition plots, from which other Dolomitic basalts evolve to higher $^{87}\text{Sr}/^{86}\text{Sr}$ values at near-constant $^{206}\text{Pb}/^{204}\text{Pb}$. The high Sr content, high $^{87}\text{Sr}/^{86}\text{Sr}$ and low Pb content expected for the Permo-Triassic carbonates suggest that these $^{87}\text{Sr}/^{86}\text{Sr}$ variations at virtually constant $^{206}\text{Pb}/^{204}\text{Pb}$ could be related to contamination by carbonates during magma emplacement. This is also supported by the composition of sample FC18, which shows the highest $^{87}\text{Sr}/^{86}\text{Sr}_i$ and crops out close to the Monzoni area, where there is evidence of widespread carbonate–magma interaction.

The fact that the lamprophyre dyke PR107, which cuts the mineralized volcanics of the Bedovina mine, shows Pb isotopic ratios similar to the host rocks (Fig. 8), could suggest contamination of the lamprophyres by Pb-rich hydrothermal fluids. However, its PM-normalized trace-element pattern shows a negative Pb anomaly, in contrast with possible contamination by Pb-rich fluids. It is therefore more likely that the Pb isotopic feature of the lamprophyres was inherited from the mantle source.

Based on Sr, Nd and Pb isotope data, we therefore suggest that magma–crust interaction in the Dolomites was limited to <5% of carbonate contamination for the basaltic lava flows, dykes and sills, and could reach up to 10% for the plutonic complex of Mount Monzoni. Similar values have been suggested by Casetta *et al.* (2018a) for the Predazzo intrusive complex. No significant interaction with silicic crustal material is required. On the other hand, in the Carnic Alps the rare basaltic magmas instead record contamination by silicic crust, which could have reached 20%. We note that this high value does not necessarily imply 20% of assimilation of crustal material and can also be related to an inappropriate initial assumption regarding the composition of the host rocks in which the magmas were emplaced.

A possible schematic model that would explain the differences between the magmas of the Dolomites and those of the Carnic–Julian areas is shown in Figure 11. Since the crust of the Dolomitic area suffered large amounts of acid magma extraction during the Permian period (i.e. Brixen granite, Cima d’Asta granite and the Atesina

intermediate–acidic explosive and effusive volcanic products; Bellieni *et al.* 2010; Fig. 1), it is reasonable to assume that the local crust was geochemically depleted and refractory during the Triassic period. This would explain not only the irrelevant or minor silicic contamination of the basaltic magmas in the Dolomitic area, but also the scarce acid magmatic manifestations in the Dolomitic area, represented only by the Predazzo granite, a small sub-intrusive complex cropping out at the boundary of the Monzoni area (Casetta *et al.* 2018a, b). Notably, this contrasts with the evolution of the Carnic–Julian Alps, where there is no evidence of melting events in Permian times; the presence of a fertile crust during the Triassic period is therefore more likely. This would in turn explain the higher degree of silicic contamination recorded in the rare basaltic lava flows and the predominance of acidic–pyroclastic manifestations in this area.

10.c. Characteristics of the mantle source(s)

Despite the absence of primary basalts, some geochemical features of the basaltic suite from the Dolomites can still give relevant information about the nature of the mantle source(s). The high-pressure and -temperature melting experiments of Conceição & Green (2004) demonstrate that shoshonitic melts can be produced by decompression melting of phlogopite- and pargasite-bearing lherzolites at P c. 1–2 GPa and T in the range 1050–1150°C. No robust experimental constraints are known for the genesis of amphibole-bearing lamprophyres, but previous work suggests that similar magmas might originate by low-degree melting of similar mantle domains, but at higher pressures (≥ 3 GPa), possibly at the asthenosphere–lithosphere boundary (Foley, 1990; Tappe *et al.* 2006). This boundary marks the transition between a porous and a channelized flow regime where fluid-rich melts may be forced to crystallize because of their low heat capacity (Tappe *et al.* 2006).

The PM-normalized trace-element compositions of the basaltic suite indicate that their mantle source was enriched in LILE, LREE and volatiles. The Sr and Nd isotopic data of the less-contaminated

samples of the basaltic suite and lamprophyres plot from MORB towards EMI-like composition. In addition, the Pb isotopic data suggest an enrichment in EMII or GLOSS components (Fig. 8). These isotopic compositions could have been acquired by interaction of the source with fluids derived by possible underlying subducting slab, as also suggested by the negative Nb anomalies and positive Pb anomalies. On the other hand, the lamprophyres show no Nb anomalies in multi-element PM-normalized diagrams (Fig. 6). Experimental work shows that the partition coefficient of Nb between slab-derived fluids and clinopyroxene is very low at pressures of 1–2 GPa, but increases at higher pressures (Baier *et al.* 2008). This means that the relative Nb content in the metasomatized mantle section would increase with pressure. This might explain the difference in negative anomalies between the basaltic suite and the lamprophyres, which likely generated at pressures of 1–2 GPa and >3 GPa, respectively.

Given these considerations, we speculate that possible mantle-type sources of these magmas are the phlogopite- and phlogopite+amphibole-bearing peridotites similar to those from the Finero and Ulten complexes (Fig. 1; Zanetti *et al.* 1999; Tumati *et al.* 2003; Scambelluri *et al.* 2010). It is worth noting that the metasomatism in the Finero peridotites is believed to have occurred during the Variscan orogenesis, and the Ulten complex is considered the mantle wedge associated with a subduction that occurred during the same orogenesis, that is, about 100 Ma before the Carnian magmatism in the Southern Alps.

Casetta *et al.* (2019) suggest that the magmatic (lamprophyric and basaltic) pulses at *c.* 220 Ma represent a transition to a mantle source less contaminated by subducted components with respect to magmatism at *c.* 235 Ma. This interpretation is based on: (1) the depleted isotopic signature of the Predazzo lamprophyre (*c.* 220 Ma) with respect to Predazzo intrusive complex magmas (*c.* 235 Ma); (2) the presence of a negative Nb anomaly in the Predazzo intrusive complex magmas and the absence of the same anomaly in the lamprophyres; and (3) the fact that the *c.* 220 Ma basaltic rocks from Brescian Alps indicate a tholeiitic affinity according to Cassinis *et al.* (2008). However, these three arguments do not consider that: (1) the lamprophyre from Marmolada (our sample DO123), which shows generally similar geochemical composition and might be coeval with the Predazzo lamprophyres, shows a more enriched isotopic signature, plotting close to the less-contaminated samples of the Basaltic suite (in addition, the *c.* 238 Ma basic rocks from Karawanke also plot in the depleted isotopic field); (2) Nb negative anomalies are present in the samples of both magmatic pulses (*c.* 220 Ma and *c.* 235 Ma; Visonà & Zanferrari, 2000; De Min *et al.* 2009; Miller *et al.* 2011; see also Fig. 6); and (3) the tholeiitic affinity of the samples at *c.* 220 Ma does not require a source that is more depleted, but can also be explained by melting at shallow pressure by lithospheric thinning, which could be consistent with an incipient extensive system.

10.d. On the geodynamic setting of Triassic magmatism in the Southern Alps

In the light of the recent literature and the new data presented in this work, we discuss the two main geodynamic scenarios suggested for the origin of Triassic magmatism in Southern Alps and propose a possible solution.

10.d.1. A Triassic back-arc is not required in northern Adria

The hypothesis of a back-arc at the margins of the Adria Plate during the Permian and Triassic periods has mainly been driven

by the suggested presence of a N-wards subduction south of Adria (Fig. 2a), high subsidence rates recorded in the Triassic sedimentary units of the Dolomites and the geochemical affinity of some of the magmatic rocks with present-day subduction-related products (Stampfli *et al.* 2002, 2003; Armienti *et al.* 2003; Csontos & Vörös, 2004; Stampfli, 2005; Doglioni & Carminati, 2008; Zanetti *et al.* 2013).

The lines of evidence for a subduction of the Palaeotethys south of Adria during the Triassic period are scarce and poorly constrained. The main evidence used by Stampfli *et al.* (2003) and Csontos & Vörös (2004) is the occurrence of pelagic sediments from the Sicilian basin in Sicily (e.g. Catalano *et al.* 1991). These sediments, despite possibly testifying the presence of the Palaeotethys south of Adria during the Triassic period, do not imply its subduction. Based on the more recent work of Schettino & Turco (2011), this oceanic sector (Ionian Basin in Fig. 2a) was a closed oceanic remnant that did not undergo any subduction in the Triassic period. For Csontos & Vörös (2004), other lines of evidence for a subduction are the suspect occurrence of a turbidite in the High Karst platform (Aubouin *et al.* 1970) and the occurrence of Triassic calc-alkaline volcanism in the Dinaric and Hellenic chain. The latter cannot be used as proof of a subduction; some other authors (Pamić, 1984; Pe-Piper, 1998) actually related this volcanism to the Triassic intra-Pangea rifting. More importantly, in the area around Adria there is no solid evidence, such as ophiolite masses, accretionary prisms, metamorphism or diffuse intermediate (andesitic) magmatism, for a subduction in the Triassic period. The closest findings are some fore-arc-type sequences found in Crete and Turkey (Stampfli *et al.* 2003).

The high subsidence rate (600 m Ma^{-1}) recorded in the Triassic units of the Dolomites (Goldhammer *et al.* 1990) has been suggested to be indicative of back-arc basins (Doglioni & Carminati, 2008). However, along the eastern coast of the USA and in western Morocco, subsidence rates reached up to $c. 800 \text{ m Ma}^{-1}$ during the Upper Triassic period in a clearly extensional setting related to the break-up of Pangea (cf. Olsen, 1997; Olsen *et al.* 2003). This implies that high subsidence rates may also be associated with the development of passive margins and therefore cannot be used as evidence of a back-arc basin.

The main geochemical features of the magmas that led some authors (e.g. Castellarin *et al.* 1988; Stampfli *et al.* 2002; Armienti *et al.* 2003; Doglioni & Carminati, 2008) to suggest a coeval subduction are the shoshonitic affinity and the negative Nb and Ti anomalies shown in PM-normalized trace-element patterns. To draw their interpretations, these authors considered such features as ubiquitous, but this is not the case for the Southern Alps and Alcapa. They are indeed not shown by the coeval Karawanke basic igneous rocks (e.g. Miller *et al.* 2011). Moreover, the *c.* 15 Ma younger magmatic rocks show either negative (basaltic rocks from the Adriatic domain; De Min *et al.* 2009) or positive Nb v. La anomalies (Dolomitic lamprophyres in this work and in Casetta *et al.* 2019). In addition, the shoshonitic affinity and Nb and Ti anomalies do not necessarily imply a coeval subduction (Müller *et al.* 1992; Li *et al.* 2015). For example, magmatic products similar to the Triassic units from the Dolomites are also found associated with extensional tectonic regimes emplaced on mobile belts that underwent subduction events in the past (e.g. Comin-Chiaromonte *et al.* 1997; De Min *et al.* 2018).

The recent database used by Li *et al.* (2015) to test the reliability of tectono-magmatic diagrams has been used here to determine whether the Triassic igneous rocks from the Southern Alps and Alcapa show any affinity with back-arc magmatism. For consistency

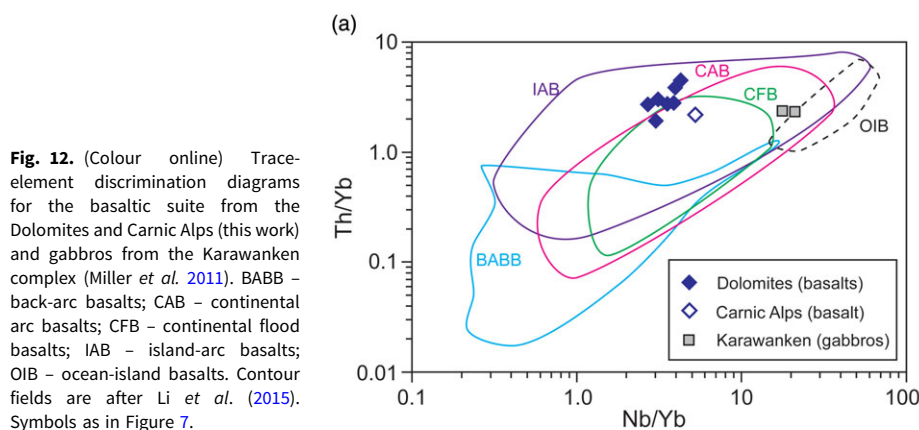


Fig. 12. (Colour online) Trace-element discrimination diagrams for the basaltic suite from the Dolomites and Carnic Alps (this work) and gabbros from the Karawanken complex (Miller *et al.* 2011). BABB – back-arc basalts; CAB – continental arc basalts; CFB – continental flood basalts; IAB – island-arc basalts; OIB – ocean-island basalts. Contour fields are after Li *et al.* (2015). Symbols as in Figure 7.

with this database, we plotted only the basaltic and gabbroic samples with MgO > 4 wt%. Figure 12 shows the results for the Zr–Y–Ti and the Th/Yb v. Nb/Yb diagrams, in which the fields for some tectonic settings defined by Li *et al.* (2015) are reported. Despite the large overlap between these fields, the results indicate that none of the samples considered here plot in the fields defined by back-arc basalts. In both diagrams, the closest similarities to our samples are with either island-arc basalts or continental-arc basalts. Given that the extensional tectonics and the high subsidence and sedimentation rates in the Dolomites during the Triassic period are not compatible with an active subduction underneath the study area, these trace-element signatures must have been inherited from some previous subduction event affecting the mantle source of the magmas. These results not only confirm that a back-arc setting is not required to explain the geochemistry of the magmas, but even suggest that this is the less-probable geodynamic setting that would produce magmas with the observed trace-element features.

10.d.2. Triassic magmatism as an early stage of Pangea break-up

The available geological and petrological evidence leads us to suggest that the Triassic magmatism from the Southern Alps did not emplace in an arc or a back-arc setting. Rather, it was likely triggered by the extensional and transtensional tectonics related to the same rifting system that superimposed the intra-Pangea dextral shear (Muttoni *et al.* 2009), and later caused the opening of the Alpine Tethys (e.g. Bortolotti & Principi, 2005; Schettino & Turco, 2011) and the break-up of Pangea during Early Jurassic time (Olsen, 1997; Schliche *et al.* 2003; Fig. 13). The subduction signatures of the magmas (Figs 6, 12) were probably inherited from the subduction events that occurred during the Variscan or even older orogenic cycles (Greenvillian?), as already suggested by some other authors (Crisci *et al.* 1984; Sloman, 1989; Bonadiman *et al.* 1994; Beccaluva *et al.* 2005; Lustrino *et al.* 2019). This interpretation is supported by the model ages ($T_{DM}(Nd)$) calculated in this work (345–1200 Ma) and the geochemistry and ages of zircons collected in the middle-Triassic volcanoclastics in the Southern and Eastern Alps (Beltràn-Triviño *et al.* 2016). In addition, the Finero and Ulten peridotites (Fig. 1), which might represent a source type for the basaltic suite in the Southern Alps, show evidence of Variscan subduction events at the northern margin of Adria (Zanetti *et al.* 1999; Tumiat *et al.* 2003; Scambelluri *et al.* 2010).

Following the review of Beccaluva *et al.* (2005) and the plate reconstructions of Schettino & Turco (2011), we suggest that the Upper Triassic rifting events in southern Europe could explain not only the Triassic magmatism in the Southern Alps, but also

the coeval magmatism in Sardinia, western Alcaipa and Dinarides, and possibly the Calabrian–Peloritani unit. These were all located at the margins of Adria during Triassic time and they all possibly represent magmatic episodes associated with first incipient rifting along these margins. The suggested palaeogeographic positions of these magmatic suites and their relations with the main geodynamic events are tentatively drawn in Figure 13. Such a scenario does not imply similar geochemical affinities and mantle sources for all the erupted magmas, since the different sectors of the Adria lithosphere might have been affected by different processes during the previous tectono-magmatic events (e.g. Visonà & Zanferrari, 2000).

Age data of the magmatic products at the margins of Adria constrain the peak of the magmatic activity to 242–235 Ma (e.g. Cassinis & Zezza, 1982; Pamić, 1984; Vaccaro *et al.* 1991; Laurenzi *et al.* 1994; Visonà & Zanferrari, 2000; Stähle *et al.* 2001; Liberi *et al.* 2011; Zanetti *et al.* 2013; Beltràn-Triviño *et al.* 2016; Storck *et al.* 2019), with minor pulses at about 215–220 Ma (e.g. Stähle *et al.* 2001; Cassinis *et al.* 2008; Casetta *et al.* 2019) and 192–187 Ma (Galli *et al.* 2019). However, U–Pb zircon ages of the deep crustal intrusions from Finero (e.g. Zanetti *et al.* 2013; Schaltegger *et al.* 2015; Langone *et al.* 2017, 2018) show that, at least in some regions, the lower crust at the margins of Adria was affected by a long-lasting cycle of heating pulses from early Permian to Early Jurassic time. These pulses were coeval with the widespread extensional tectonics recorded all over Adria (e.g. Bortolotti & Principi, 2005). The peak age of the magmatic events, the long-lasting heating and thinning cycle, and the position of Adria in the Pangea supercontinent all suggest that Triassic magmatism at the margins of Adria is an expression of a major loss of heat accumulated beneath Pangea since its amalgamation. Based on Veevers (1989), such a loss of heat occurred at 230 ± 5 Ma.

As shown by Schettino & Turco (2011), the rifting on the northeastern margin of Adria (i.e. Dinarides, Southern Alps and Alcaipa) was aborted in the Jurassic period, but on the western margin it developed in a spreading centre, forming the Alpine Tethys, which was connected to the central rifting in the Atlantic (Schettino & Turco, 2011, fig. 1D) that caused the break-up of Pangea. Notably, the related Central Atlantic Magmatic Province (CAMP; peak activity at 201 Ma, average 200 Ma; Marzoli *et al.* 1999), which took place c. 30 Ma after the peak magmatic episodes around Adria, possibly extends to the northwestern margins of Adria (Fig. 13; Denyszyn *et al.* 2018). In addition, basalts of the CAMP show negative anomalies of Nb and Ti and are enriched in LILE and in isotopic composition (Callegaro *et al.* 2014, 2017; Merle *et al.* 2014; Marzoli *et al.* 2019),

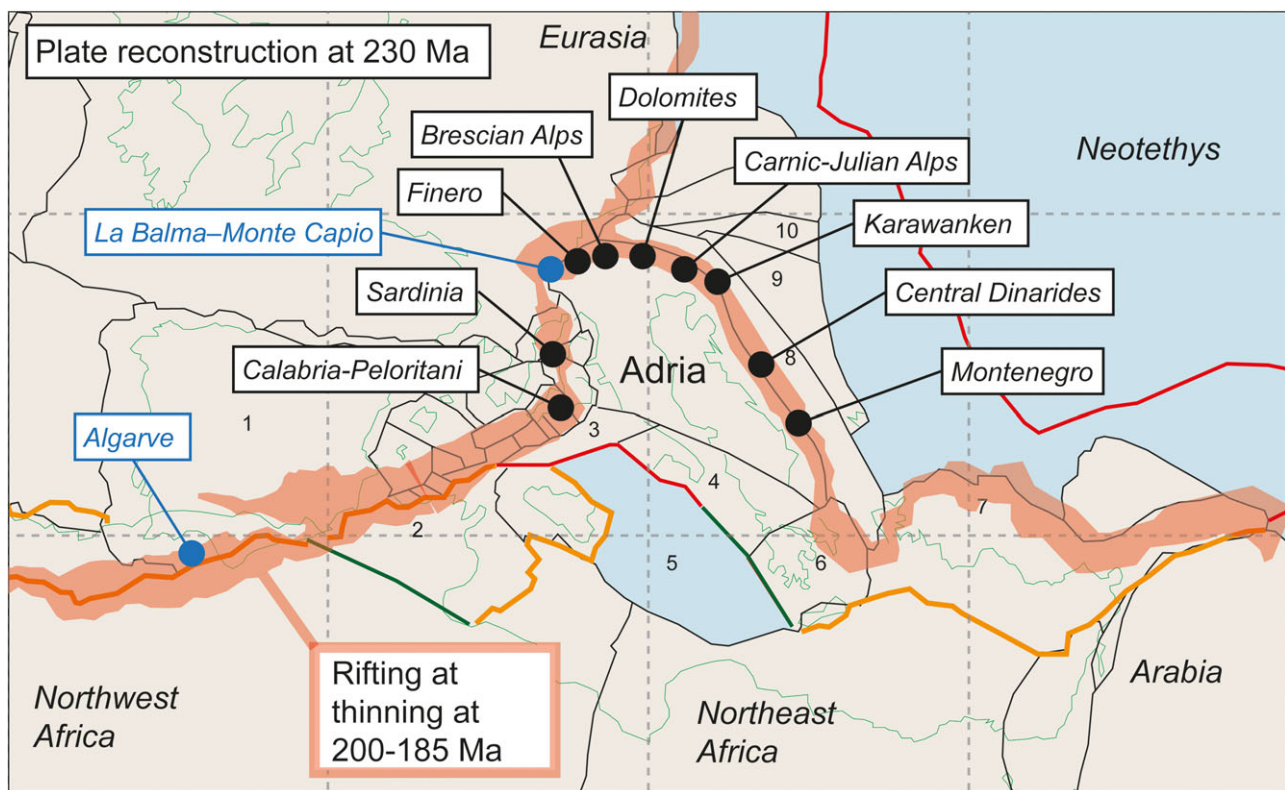


Fig. 13. (Colour online) Tentative palaeogeographical position of the Ladinian–Carnian magmatism (black circles) that today crops out in Calabria (Liberi *et al.* 2011), Sardinia (Traversa & Vaccaro, 1992), Southern and Eastern Alps (Crisci *et al.* 1984; Castellarin *et al.* 1988; Gianolla, 1992; Visonà and Zanferrari, 2000; Zanetti *et al.* 2013) and Dinarides (Pamić, 1984). Blue circles show some outcrops of the more recent (201 Ma) Central Atlantic Magmatic Province, that is, La Balma–Monte Capio, Ivrea–Verbano zone (Denyszyn *et al.* 2018) and Algarve, Spain (Callegaro *et al.* 2014). Red shaded areas show the main rifting and thinning events that occurred during 200–185 Ma (after Schettino & Turco, 2011). Note that the first rifting stages around Adria started as early as during Anisian time (e.g. Bortolotti & Principi, 2005). Plate reconstructions are after Schettino & Turco (2011). Other unit names and lines as in Figure 2.

showing some overlap with the rocks studied here. The subduction-like geochemical features are interpreted as being related to a mantle source enriched by Palaeozoic or Proterozoic subduction events (Callegaro *et al.* 2014, 2017; Merle *et al.* 2014; Marzoli *et al.* 2019). Overall, these considerations lead us to suggest that the Triassic magmatism and the associated heating pulses recorded in the lithosphere of Adria were a forerunner of the future break-up of Pangea.

11. Conclusions

The basaltic suite, lamprophyres and ignimbrites included in the Ladinian–Carnian units of the Dolomites and Carnic–Julian Alps represent part of the magmatic events that affected the northern margin of Adria in the period between the amalgamation and break-up of Pangea. Before emplacement in the upper crust and eruption to the surface, the basaltic magmas from the Dolomites underwent differentiation at depths of mostly 14–20 km, dominated by crystallization of clinopyroxene and only marginally affected by crustal contamination. Similar depths are estimated for the rare basaltic occurrences in the Carnic Alps; however, these show Sr–Nd isotopic compositions suggesting higher degrees of contamination. We infer that this difference is related to a restitic nature of the crust in the areas of the Dolomites and a more fertile crust in the Carnic–Julian Alps, which might also explain the production of Triassic rhyolites (ignimbrites) by crustal melting in the Carnic–Julian Alps only.

The shoshonitic affinity and trace-element signatures of the basaltic suite and the occurrence of lamprophyres can be explained

by different melting episodes of a mantle source that was variably metasomatized during the Variscan orogenic cycle. This supports some previous interpretations, not only for the magmatic rocks from the same localities (e.g. Sloman, 1989; Bonadiman *et al.* 1994) but also for the other outcrops in the Southern Alps (e.g. Crisci *et al.* 1984; Beccaluva *et al.* 2005; Beltràn-Triviño *et al.* 2016; Lustrino *et al.* 2019). The emplacement of coeval magmas that do not show the typical orogenic signatures for the trace elements (e.g. gabbroic intrusive complex in the Karawanken; Visonà & Zanferrari, 2000) can be explained by the presence of a heterogeneous mantle source beneath Adria. We support the view of Visonà & Zanferrari (2000), who suggested that this might reflect the complex structure of the Adriatic lithosphere, which likely formed by amalgamation of different tectonic units that underwent different geodynamic processes during the Palaeozoic era (e.g. von Raumer, 1998).

Given the above scenario and the absence of any solid geological evidence for a subduction zone in the surroundings of Adria, a back-arc setting is not required to explain the subduction-related signatures of the magmas. Rather, the widespread occurrence of extensional and transtensional tectonics, most likely connected to the Triassic–Jurassic rifting system in the central Atlantic, strongly suggests that the magmatism took place as a consequence of lithosphere thinning and mantle upwelling, which can be related to the loss of heat accumulated beneath Pangea after its amalgamation. This scenario would explain not only the origin of Triassic magmatism in the Southern Alps, but also the occurrences in Calabria, Sardinia, Karawanken and Dinarides.

Acknowledgments. We thank Lorenzo Furlan and Leonardo Tauro for sample preparation and Raul Carampin for microprobe analyses. Riccardo Petrini and Francesca Slejko are thanked for help with the thermal ionization mass spectrometry (TIMS) analyses at the University of Trieste. We thank Kathryn Goodenough for the editorial handling and two anonymous reviewers for their constructive comments. The project has been partially funded by the Italian research program PRIN 20178LPCP. Luca Ziberna acknowledges the Alexander von Humboldt Foundation.

Supplementary material. To view supplementary material for this article, please visit <https://doi.org/10.1017/S0016756820000084>

References

- Abbas H, Michail M, Cifelli F, Mattei M, Gianolla P, Lustrino M and Carminati E (2018) Emplacement modes of the Ladinian plutonic rocks of the Dolomites: insights from anisotropy of magnetic susceptibility. *Journal of Structural Geology* **113**, 42–61.
- Armienti P, Corazzato C, Gropelli G, Natoli E and Pasquare G (2003) Geological and petrographical study of Montecampione Triassic subvolcanic bodies (Southern Alps, Italy): preliminary geodynamic results. *Bollettino della società Geologica Italiana*, Volume Speciale **2**, 67–78.
- Artioli G, Angelini I, Nimis P and Villa IM (2016) Lead-isotope database of copper ores from the Southeastern Alps: a tool for the investigation of pre-historic copper metallurgy. *Journal of Archaeological Science* **75**, 27–39.
- Aubouin J, Blanchet R, Cadet P, Celet P, Charvet J, Choro-witz J, Cousin M and Rampnoux J-P (1970) Essai sur la géologie des Dinarides. *Bulletin de la Société Géologique de France* **12**, 1060–95.
- Baier J, Audétat A and Keppler H (2008) The origin of the negative niobium tantalum anomaly in subduction zone magmas. *Earth and Planetary Science Letters* **267**, 290–300.
- Baker J, Peate D, Waight T and Meyzen C (2004) Pb isotopic analysis of standards and samples using a 207Pb–204Pb double spike and thallium to correct for mass bias with a double-focusing MC-ICPMS. *Chemical Geology* **211**, 275–303.
- Beccaluva L, Coltorti M, Saccani E, Siena F and Zeda O (2005) Triassic magmatism and Jurassic ophiolites at the margins of the Adria Plate. In *CROP PROJECT: Deep Seismic Exploration of the Central Mediterranean and Italy* (ed IR Finetti), pp. 607–21. Amsterdam: Elsevier.
- Beguelin P, Chiaradia M, Beate B and Spikings RA (2015) The Yanaurcu volcano (Western Cordillera, Ecuador): a field, petrographic, geochemical, isotopic and geochronological study *Lithos* **218–219**, 37–53.
- Bellieni G, Fioretti AM, Marzoli A and Visonà D (2010) Permo–Paleogene magmatism in the eastern Alps. *Rendiconti Lincei* **21**, 51–71.
- Beltrán-Triviño A, Winkler W, Von Quadt A and Gallofer D (2016) Triassic magmatism on the transition from Variscan to Alpine cycles: evidence from U–Pb, Hf, and geochemistry of detrital minerals. *Swiss Journal of Geosciences* **109**, 309–28.
- Beltrando M, Stockli DF, Decarli A and Manatschal G (2015) A crustal-scale view at rift localization along the fossil Adriatic margin of the Alpine Tethys preserved in NW Italy. *Tectonics* **34**, 1927–51.
- Bianchi A and Di Cobertaldo D (1956) Osservazioni paragenetiche sul giacimento a rame e tungsteno della Bedovina presso Predazzo. *Rendiconti SMI* **12**, 55–65.
- Bianchini G, Natali C, Shibata T and Yoshikawa M (2018) Basic dykes cross-cutting the crystalline basement of Valsugana (Italy): new evidence of Early Triassic volcanism in the Southern Alps. *Tectonics* **37**, 2080–93.
- Bole M, Dolenc T, Zupančič N and Činč-Juhant B (2001) The Karawanke Granitic Belt (Slovenia) – a bimodal Triassic alkaline plutonic complex. *Schweizerische Mineralogische Petrographische Mitteilungen* **81**, 23–38.
- Bonadiman C, Coltorti M and Siena F (1994) Petrogenesis and T–fO₂ estimates of Mt. Monzoni complex (Central Dolomites, Southern Alps): a Triassic shoshonitic intrusion in a transcurrent geodynamic setting. *European Journal of Mineralogy* **6**, 943–66.
- Borsi S and Ferrara G (1968) Isotopic age measurements of the M. Monzoni intrusive complex. *Minerologica et Petrographica Acta* **14**, 171–83
- Bortolotti V and Principi G (2005) Tethyan ophiolites and Pangea break-up. *The Island Arc* **14**, 442–70.
- Boynton WV (1984) Geochemistry of rare Earth elements: meteorite studies. In *Rare Earth Element Geochemistry* (ed P. Henderson), pp. 63–114. Amsterdam: Elsevier.
- Callegaro S, Marzoli A, Bertrand H, Bichert-Toft J, Reisberg L, Cavazzini G, Jourdan F, Davies J HFL, Parisio L, Bouchet R, Paul A, Schaltegger U and Chiaradia M (2017) Geochemical constraints provided by the Freetown Layered Complex (Sierra Leone) on the origin of high-ti tholeiitic CAMP magmas. *Journal of Petrology* **58**, 1811–40.
- Callegaro S, Rapaille C, Marzoli A, Bertrand H, Chiaradia M, Reisberg L, Bellieni G, Martins L, Madeira J, Mata J, Youbi N, De Min A, Azevedo MR and Bensalah MK (2014) Enriched mantle source for the Central Atlantic magmatic province: New supporting evidence from southwestern Europe. *Lithos* **188**, 15–32.
- Carraro A and Visonà D (2003) Mantle xenoliths in Triassic camptonite dykes of the Predazzo Area (Dolomites, Northern Italy): petrography, mineral chemistry and geothermobarometry. *European Journal of Mineralogy* **15**, 103–15.
- Casetta F, Coltorti M, Ickert RB, Bonadiman C, Giacomoni PP and Ntaflou T (2018a) Intrusion of shoshonitic magmas at shallow crustal depth: T–P path, H₂O estimates, and AFC modeling of the Middle Triassic Predazzo Intrusive Complex (Southern Alps, Italy). *Contributions to Mineralogy and Petrology* **173**, 57.
- Casetta F, Coltorti M and Marocchino E (2018b) Petrological evolution of the Middle Triassic Predazzo Intrusive Complex, Italian Alps. *International Geology Review* **60**, 977–97.
- Casetta F, Ickert RB, Mark DF, Bonadiman C, Giacomoni PP, Ntaflou T and Coltorti M (2019) The alkaline lamprophyres of the Dolomitic area (Southern Alps, Italy): markers of the Late Triassic change from orogenic-like to anorogenic magmatism. *Journal of Petrology* **60**, 1263–98.
- Cassinis G, Cortesogno L, Gaggero L, Perotti CR and Buzzi L (2008) Permian to Triassic geodynamic and magmatic evolution of the Brescian Prealps (eastern Lombardy, Italy). *Bollettino della Società Geologica Italiana* **127**, 501–18.
- Cassinis G and Zezza U (1982) Dati geologici e petrografici sui prodotti del magmatismo triassico nelle Prealpi Bresciane. In *Guida alla Geologia del Sudalpino Centro-orientale* (eds A. Castellarin and GB Vai), pp. 157–71. Siena: Guide Geologiche Regionali SGI.
- Castellarin A, Lucchini F, Rossi PL, Selli L and Simboli G (1988) The Middle Triassic magmatic-tectonic arc development in the Southern Alps. *Tectonophysics* **146**, 79–89.
- Catalano R, Di Stefano P and Kozur H (1991) Permian circum-pacific deep-water faunas from the Western Tethys (Sicily-Italy) – new evidences for the position of the Permian Tethys. *Palaeogeography, Palaeoclimatology, Palaeoecology* **87**, 75–108.
- Chiaradia M, Müntener O and Beate B (2011) Enriched basaltic andesites from mid-crustal fractional crystallization, recharge, and assimilation (Pilavo Volcano, Western Cordillera of Ecuador). *Journal of Petrology* **52**, 1107–41.
- Comin-Chiaromoniti P, Cundari A, Piccirillo EM, Gomes CB, Castorina F, Censi P, De Min A, Marzoli A, Speziale S and Velázquez VF (1997) Potassic and sodic igneous rocks from eastern Paraguay: their origin from the lithospheric mantle and genetic relationships with the associated Paraná flood tholeiites. *Journal of Petrology* **38**, 495–528.
- Conceição RV and Green DH (2004) Derivation of potassic (shoshonitic) magmas by decompression melting of phlogopite+argasite lherzolite. *Lithos* **72**, 209–29.
- Crisci CM, Ferrara G, Mazzuoli R and Rossi PM (1984) Geochemical and geochronological data on Triassic volcanism of the Southern Alps of Lombardy (Italy): genetic implications. *Geologische Rundschau* **73**, 279–92.
- Cross W, Iddings JP, Pirsson LV and Washington HS (1902) A quantitative-chemico-mineralogical classification and nomenclature of igneous rocks. *Journal of Geology* **10**, 555–693.
- Csontos L and Vörös A (2004) Mesozoic plate tectonic reconstruction of the Carpathian region. *Palaeogeography, Palaeoclimatology, Palaeoecology* **210**, 1–56.
- de la Roche H, Leterrier J, Grandclaude P and Marchal M (1980) A classification of volcanic and plutonic rocks using R1R2-diagram and major-element analyses – its relationships with current nomenclature. *Chemical Geology* **29**, 183–210.

- De Min A, Callegaro S, Marzoli A, Nardy AJ, Chiaradia M, Marques L and Gabbarrini I (2018) Insights into the petrogenesis of low- and high-Ti basalts: stratigraphy and geochemistry of four lava sequences from the central Paraná basin. *Journal of Volcanology and Geothermal Research* **355**, 232–52.
- De Min A, Jourdan F, Marzoli A, Renne PR and Juračić M (2009) The tholeiitic magmatism of Jabuka, Vis and Brusnik islands: a Carnian magmatism in the Adria Plate. *Rendiconti online della Società Geologica Italiana* **9**, 85.
- De Vecchi GP and Sedeo R (1983) Il vulcanesimo medio-triassico nelle Prealpi Vicentine (Italia Settentrionale). *Memorie di Scienze Geologiche* **36**, 149–69.
- Denyszyn SW, Fiorentini ML, Maas R and Dering G (2018) A bigger tent for CAMP. *Geology* **46**, 823–26.
- DePaolo DJ (1981) Trace elements and isotopic effect of combined wallrock assimilation and fractional crystallization. *Earth and Planetary Science Letters* **53**, 189–202.
- Dogliani C (1987) Tectonics of the Dolomites (Southern Alps, Northern Italy). *Journal of Structural Geology* **9**, 181–93.
- Dogliani C and Carminati E (2008) Structural styles and Dolomites field trip. *Memorie Descrittive della Carta Geologica Italiana* **82**, 299 pp.
- Dorozi R, Vaccaro C, Masoudi F and Petrini R (2016) Cretaceous alkaline volcanism in south Marzanabad, northern central Alborz, Iran: geochemistry and petrogenesis. *Geoscience Frontiers* **7**, 937–51.
- Faure G, Assereto R and Tremba EL (1978) Strontium isotope composition of marine carbonates of Middle Triassic to Early Jurassic age, Lombardic Alps, Italy. *Sedimentology* **25**, 523–43.
- Foley S (1990) A review and assessment of experiments on kimberlites, lamproites and lamprophyres as a guide to their origin. *Proceedings of the Indian Academy of Science* **99**, 57–80.
- Furrer H, Shaltegger U, Ovtchanova M and Meiste P (2008) U–Pb zircon age of volcanoclastic layers in Middle Triassic platform carbonates of the Austroalpine Silvretta nappe (Switzerland). *Swiss Journal of Geosciences* **101**, 595–603.
- Galli A, Grassi D, Sartori G, Gianola O, Burg J-P and Schmidt MW (2019) Jurassic carbonatite and alkaline magmatism in the Ivrea zone (European Alps) related to the breakup of Pangea. *Geology* **47**, 199–202.
- Gasparotto G and Simboli G (1991) Mineralogia, petrografia e schemi evolutivi delle magmatiti triassiche del complesso di Cima Pape (Dolomiti Orientali). *Mineralogica et Petrografica Acta* **34**, 205–34.
- Gianola P (1992) Evoluzione Mediotriassica del Vulcanesimo di Rio Freddo. *Memorie di Scienze Geologiche* **19**, 193–209.
- Gianola P, De Zanche P and Mietto P (1998) Triassic sequence stratigraphy in the Southern Alps (northern Italy): Definition of sequences and basin evolution. In *Mesozoic and Cenozoic Sequence Stratigraphy of European Basins*, pp. 719–47. SEPM Society for Sedimentary Geology, Special Publication no. 60.
- Goldhammer RK, Dunn PA and Hardie LA (1990) Depositional cycles, composite sea-level changes, cycle stacking patterns, and the hierarchy of stratigraphic forcing. *Geological Society of America Bulletin* **102**, 535–62.
- Golonka J (2004) Plate tectonic evolution of the southern margin of Eurasia in the Mesozoic and Cenozoic. *Tectonophysics* **381**, 235–73.
- Grocke SB, Cottrell E, de Silva S and Kelley KA (2016) The role of crustal and eruptive processes versus source variations in controlling the oxidation state of iron in Central Andean magmas. *Earth and Planetary Science Letters* **440**, 92–104.
- Handy HR, Franz L, Heller F, Janott B and Zurbriegen R (1999) Multistage accretion and exhumation of the continental crust (Ivrea crustal section, Italy and Switzerland). *Tectonics* **18**, 1154–77.
- Hart S and Zindler A (1989) Constraints on the nature and development of chemical heterogeneities in the mantle. In *Mantle Convection* (ed. WR Peltier), pp. 216–387. New York: Gordon and Breach Science Publishers.
- Hart SR (1984) A large scale isotope anomaly in the Southern Hemisphere mantle. *Nature* **309**, 753–57.
- Koppel V and Schroll E (1988) Pb-isotope evidence for the origin of lead in strata-bound Pb–Zn deposits in Triassic carbonates of the Eastern and Southern Alps. *Mineralium Deposita* **23**, 96–103.
- Korte C, Kozur HW, Bruckschen P and Veizer J (2003) Strontium isotope evolution of Late Permian and Triassic seawater. *Geochimica et Cosmochimica Acta* **67**, 47–62.
- Kozur H (1991) The evolution of the Meliata–Hallstatt Ocean and its significance for the early evolution of the Eastern Alps and Western Carpathians. *Palaeogeography, Palaeoclimatology, Palaeoecology* **87**, 109–35.
- Lago M, Arranz E, Pocovi A, Galé C and Gil-Imaz A (2004) Permian magmatism and basin dynamics in the southern Pyrenees: a record of the transition from late Variscan transtension to early Alpine extension. In *Permo-Carboniferous Magmatism and Rifting in Europe* (eds M Wilson, E-R Neumann, GR Davies, MY Timmerman, M Heeremans and BT Larsen), pp. 439–64. Geological Society of London, Special Publication no. 223.
- Lange RA, Frey HM and Hector J (2009) A thermodynamic model for the plagioclase-liquid hygrometer/thermometer. *American Mineralogist* **94**, 494–506.
- Langone A, Padrón-Navarta José A, Ji W-Q, Zanetti A, Mazzucchelli M, Tiepolo M, Giovanardi T and Bonazzi M (2017) Ductile–brittle deformation effects on crystal-chemistry and U–Pb ages of magmatic and metasomatic zircons from a dyke of the Finero Mafic Complex (Ivrea–Verbano Zone, Italian Alps). *Lithos* **284–85**, 493–511.
- Langone A, Zanetti A, Daczko NR, Piazzolo S, Tiepolo M and Mazzucchelli M (2018) Zircon U–Pb dating of a lower crustal shear zone: a case study from the northern sector of the Ivrea–Verbano Zone (Val Cannobina, Italy). *Tectonics* **37**, 322–42.
- Laurenzi MA and Visonà D (1996) 40Ar/39Ar Chronology of Predazzo magmatic complex (Southern Alps, Italy). In *Proceedings of 78th Riunione estiva Società Geologica Italiana, Geologia delle Dolomiti*, 16–18 September 1996, San Cassiano di Val Badia (BZ), Italy.
- Laurenzi MA, Visonà D and Zantedeschi C (1994) High resolution Ar/Ar chronology of Predazzo magmatic complex (Southern Alps, Italy). *ICOG* **8**, 5–11.
- Le Bas MJ, Le Maitre RW and Woolley AR (1992) The construction of the Total Alkali–Silica chemical classification of volcanic rocks. *Mineralogy and Petrology* **46**, 1–22.
- Le Maitre RW, Streckeisen A, Zanettin B, Le Bas MJ, Bonin, B, Bateman P (2002) *Igneous Rocks. A Classification and Glossary of Terms. Recommendations of the IUGS Subcommittee on the Systematics of Igneous Rocks*. Cambridge University Press, Cambridge.
- Leake BE, Woolley AR, Arps CES, Birch WD, Gilbert MC, Grice JD, Hawthorne FC and Youzhi G (1997) Nomenclature of amphiboles: report of the subcommittee on amphiboles of the international mineralogical association, commission on new minerals and mineral names. *American Mineralogist* **82**, 1019–37.
- Li C, Arndt TN, Tang Q and Ripley ME (2015) Trace element indiscrimination diagrams. *Lithos* **232**, 76–83.
- Liberi F, Piluso E and Langone A (2011) Permo-Triassic thermal events in the lower Variscan continental crust section of the Northern Calabrian Arc, Southern Italy: insights from petrological data and in situ U–Pb zircon geochronology on gabbros. *Lithos* **124**, 291–307.
- Lu M, Hofmann AW, Mazzucchelli M and Rivalenti G (1997a) The mafic-ultramafic complex near Finero (Ivrea–Verbano Zone), II. Geochronology and isotope geochemistry. *Chemical Geology* **140**, 223–35.
- Lu M, Hofmann AW, Mazzucchelli M and Rivalenti G (1997b) The mafic-ultramafic complex near Finero (Ivrea–Verbano Zone), I. Chemistry of MORB-like magmas. *Chemical Geology* **140**, 207–22.
- Lucchini F and Morten L (1977) An example of flow differentiation: clinopyroxene of the Predazzo igneous complex (north Italy). *Lithos* **10**, 39–47.
- Lustrino M, Abbas H, Agostini S, Caggiati M, Carminati E and Gianola P (2019) Origin of Triassic magmatism of the Southern Alps (Italy): constraints from geochemistry and Sr–Nd–Pb isotopic ratios. *Gondwana Research* **75**, 218–38.
- Marzoli A, Bertrand H, Youbi N, Callegaro S., Merle RE, Reisberg L, Chiaradia M, Sarah B, Jourdan F, Zanetti A, Davies J, Cuppone T, Mahmoudi A, Medina F, Renne P, Bellieni G, Crivellari S, Hachimi HE, Bensalah MK, Meyzen C and Tegner C (2019) The Central Atlantic Magmatic Province (CAMP) in Morocco. *Journal of Petrology* **60**, 945–96.

- Marzoli A, Renne PR, Piccirillo EM, Ernesto M, Bellieni G and De Min A** (1999) Extensive 200-million-year-old continental flood basalts of the Central Atlantic Magmatic Province. *Science* **284**, 616–18.
- McDonough WF and Sun SS** (1995) The composition of the Earth. *Chemical Geology* **120**, 223–53.
- Merle R, Marzoli A, Reisberg L, Bertrand H, Nemchin A, Chiaradia M, Callegaro S, Jourdan F, Bellieni G, Kontak D, Puffer J and McHone GJ** (2014) Sr, Nd, Pb and Os isotope systematics of CAMP tholeiites from Eastern North America (ENA): Evidence of a subduction-enriched mantle source. *Journal of Petrology* **55**, 133–80.
- Miller C, Thöni M, Goessler W and Tessadri R** (2011) Origin and age of the Eisenkappel gabbro to granite suite (Carinthia, SE Austrian Alps). *Lithos* **125**, 434–48.
- Miyashiro A** (1978) Nature of alkali volcanic rocks series. *Contributions to Mineralogy and Petrology* **66**, 91–104.
- Molina JF, Moreno JA, Castro A, Rodriguez C and Fershtater GB** (2015) Calcic amphibole thermobarometry in metamorphic and igneous rocks: New calibrations based on plagioclase/amphibole Al-Si partitioning and amphibole/liquid Mg partitioning. *Lithos* **232**, 286–305.
- Morimoto N** (1988) Nomenclature of pyroxenes. *Mineralogy and Petrology* **39**, 55–76.
- Moussalam Y, Oppenheimer C, Scaillet B, Gaillard F, Kyle P, Peters N, Hartley M, Berlo K and Donovan A** (2014) Tracking the changing oxidation state of Erebus magmas, from mantle to surface, driven by magma ascent and degassing. *Earth and Planetary Science Letters* **393**, 200–9.
- Müller D, Rock NMS and Groves DI** (1992) Geochemical discrimination between shoshonitic and potassic volcanic rocks in different tectonic settings: a pilot study. *Mineralogy and Petrology* **46**, 259–89.
- Muttoni G, Gaetani M, Kent DV, Sciunnach D, Angiolini L, Berra F, Garzanti E, Mattei M and Zanchi A** (2009) Opening of the Neo-Tethys Ocean and the Pangea B to Pangea A transformation during the Permian. *GeoArabia* **14**, 17–48.
- Narduzzi F, De Min A, Lenaz D and Princivalle F** (2009) Crystal-chemistry of diopsides from mantle xenoliths in the Becco di Filadonna area: equilibration pressure and petrological implications. *Rendiconti online della Società Geologica Italiana* **9**, 105–8.
- Neave DA and Putirka KD** (2017) A new clinopyroxene-liquid barometer, and implications for magma storage pressures under Icelandic rift zones. *American Mineralogist* **102**, 777–94.
- Nikishin AM, Ziegler PA, Abbott D, Brunet MF and Cloetingh S** (2002) Permo-Triassic intraplate magmatism and rifting in Eurasia: implications for mantle plumes and mantle dynamics. *Tectonophysics* **351**, 3–39.
- Olsen PE** (1997) Stratigraphic record of the early Mesozoic breakup of Pangea in the Laurasia–Gondwana rift system. *Annual Review of Earth Planetary Sciences* **25**, 337–401.
- Olsen PE, Kent DV, Et-Touhami M and Puffer J** (2003) Cyclo-, magneto-, and bio-stratigraphic constraints on the duration of the CAMP event and its relationship to the Triassic–Jurassic boundary. In *The Central Atlantic Magmatic Province; Insights from Fragments of Pangea* (eds WE Hames, JG McHone, PR Renne and CR Ruppel), pp. 7–32. Geophysical Monograph, American Geophysical Union.
- Pamić JJ** (1984) Triassic magmatism of the Dinarides in Yugoslavia. *Tectonophysics* **109**, 281–307.
- Pe-Piper G** (1998) The nature of Triassic extension-related magmatism in Greece: evidence from Nd and Pb isotope geochemistry. *Geological Magazine* **135**, 331–48.
- Pin C, Briot D, Bassin C and Poitrasson F** (1994) Concomitant separation of strontium and samarium–neodymium for isotopic analysis in silicate samples, based on specific extraction chromatography. *Analytica Chimica Acta* **298**, 209–17.
- Plank T and Langmuir CH** (1998) The chemical composition of subducting sediment and its consequences for the crust and mantle. *Chemical Geology* **145**, 325–94.
- Putirka K** (2005) Igneous thermometers and barometers based on plagioclase + liquid equilibria: Tests of some existing models and new calibrations. *American Mineralogist* **90**, 336–46.
- Putirka K** (2008) Thermometers and barometers for volcanic systems. *Reviews in Mineralogy and Geochemistry* **69**, 1–8.
- Putirka K** (2016) Amphibole thermometers and barometers for igneous systems and some implications for eruption mechanisms of felsic magmas at arc volcanoes. *American Mineralogist* **101**, 819–40.
- Quick JE, Sinigoi S, Peressini G, Demarchi G, Wooden JL and Sbisà A** (2009) Magmatic plumbing of a large Permian caldera exposed to a depth of 25 km. *Geology* **37**, 603–6.
- Rock NMS** (1987) The nature and origin of lamprophyres: an overview. In *Alkaline Igneous Rocks* (eds JG Fitton and BGJ Upton), pp. 191–226. Geological Society of London, Special Publication no. 30.
- Roeder PL and Emslie RF** (1970) Olivine-liquid equilibrium. *Contributions to Mineralogy and Petrology* **29**, 275–89.
- Rottura A, Bargossi GM, Caggianelli A, Del Moro A, Visonà D and Tranne CA** (1998) Origin and significance of the Permian high-K calc-alkaline magmatism in the central-eastern Southern Alps, Italy. *Lithos* **45**, 329–48.
- Rudnick RL and Gao S** (2003) Composition of the continental crust. In *The Crust* (ed RL Rudnick), pp. 1–64. Oxford University Press, Treatise in Geochemistry vol. 3.
- Scambelluri M, Rampone E, Braga R and Malaspina N** (2010) The Variscan garnet peridotites from the Eastern Alps (Ulten Zone): records of subduction metasomatism in the mantle wedge. *Journal of the Virtual Explorer* **36**, 28.
- Schaltegger U and Brack P** (2007) Crustal-scale magmatic systems during intracontinental strike-slip tectonics: U, Pb and Hf isotopic constraints from Permian magmatic rocks of the Southern Alps. *International Journal of Earth Science* **96**, 1131–51.
- Schaltegger U, Ulianov A, Müntener O, Ovtcharova M, Peytcheva I, Vonlanthen P, Vennemann T, Antognini M and Girlanda F** (2015) Megacrystic zircon with planar fractures in miaskite-type nepheline pegmatites formed at high pressures in the lower crust (Ivrea Zone, southern Alps, Switzerland). *American Mineralogist* **100**, 83–94.
- Schettino A and Turco E** (2011) Tectonic history of the western Tethys since the Late Triassic. *Geological Society of America Bulletin* **123**, 89–105.
- Schliche RW, Withjack MO and Olsen PE** (2003) Relative timing of CAMP, rifting, continental breakup, and basin inversion: tectonic significance. In *The Central Atlantic Magmatic Province* (eds WE Hames, GC McHone, PR Renne and C Ruppel), pp. 33–59. American Geophysical Union, Washington, Monograph no. 136.
- Schmid SM, Bernoulli D, Fügenschuh B, Matenco L, Schefer S, Schuster R, Tischler M and Ustaszewski K** (2008) The Alpine-Carpathian-Dinaric orogenic system: correlation and evolution of tectonic units. *Swiss Journal of Geoscience* **101**, 139–83.
- Schmid SM, Fügenschuh B, Kissling E and Schuster R** (2004) Tectonic map and overall architecture of the Alpine orogen. *Eclogae Geologicae Helvetiae* **97**, 93–117.
- Sengör AMC** (1984) *The Cimmeride Orogenic System and the Tectonics of Eurasia*. Geological Society of America, Special Paper no. 195, 82 pp.
- Shaw HF and Wasserburg GJ** (1985) Sm–Nd in marine carbonates and phosphates: implications for Nd isotopes in seawater and crustal ages. *Geochimica et Cosmochimica Acta* **49**, 503–18.
- Siena F and Coltorti M** (1989) The petrogenesis of a hydrated mafic–ultramafic complex and the role of amphibole fractionation at Finero (Italian Western Alps). *Neues Jahrbuch für Mineralogie* **6**, 255–74.
- Sloman LE** (1989) Triassic shoshonites from the Dolomites, Northern Italy: alkaline arc rocks in a strike-slip setting. *Journal of Geophysical Research* **94**, 4655–66.
- Stähle V, Frenzel G, Hess JC, Saube F, Schmidt ST and Schneider W** (2001) Permian metabasalt and Triassic alkaline dykes in the northern Ivrea zone: clues to the post-Variscan geodynamic evolution of the Southern Alps. *Schweizerische Mineralogische und Petrographische Mitteilungen* **81**, 1–21.
- Stampfli GM** (2005) Plate tectonic of the Apulia-Adria microcontinents. In *CROP PROJECT: Deep Seismic Exploration of the Mediterranean and Italy* (ed. IR Finetti), pp. 747–66. Elsevier, Netherlands.
- Stampfli GM and Borel GD** (2002) A plate tectonic model for the Paleozoic and Mesozoic constrained by dynamic plate boundaries and restored synthetic oceanic isochrons. *Earth and Planetary Science Letters* **196**, 17–33.

- Stampfli GM, Borel GD, Marchant R and Mosar J** (2002) Western Alps geological constraints on the western Tethyan reconstructions. In *Reconstruction of the Evolution of the Alpine-Himalayan Orogen* (eds G Rosenbaum and GS Lister), pp. 75–104. *Journal of the Virtual Explorer* 7.
- Stampfli GM, Vavassis I, De Bono A, Rosselet F, Matti B and Bellini M** (2003) Remnants of the Paleotethys oceanic suture-zone in the western Tethyan area. *Bollettino della Società Geologica Italiana, Volume Speciale* 2, 1–23.
- Storck J-C, Brack P, Worzlaw J-F and Ulmer P** (2019) Timing and evolution of Middle Triassic magmatism in the Southern Alps (northern Italy). *Journal of the Geological Society* 176, 253–68.
- Tanaka T, Togashi S, Kamioka H, Amakawa H, Kagami H, Hamamoto T, Yuhara M, Orihashi Y, Yoneda S, Shimizu H, Kunimaru T, Takahashi K, Yanagi Y, Nakano T, Fujimaki H, Shinjo R, Asahara Y, Tanimizu M and Dragusanu C** (2000) JNdi-1: a neodymium isotopic reference in consistency with La Jolla neodymium. *Chemical Geology* 168, 279–81.
- Tappe S, Folet SF, Jenner GA, Heaman LM, Kjarsgaard BA, Romer RL, Stracke A, Joyce N and Hoefs J** (2006) Genesis of ultramafic lamprophyres and carbonatites at Aillik Bay, Labrador: a consequence of incipient lithospheric thinning beneath the North Atlantic Craton. *Journal of Petrology* 47, 1261–315.
- Traversa G and Vaccaro C** (1992) REE distribution in the late Hercynian dykes from Sardinia. *IGCP Project No. 276, Newsletter* 5, 215–226.
- Tumiati S, Thöni M, Nimis P, Martin S and Mair V** (2003) Mantle–crust interactions during Variscan subduction in the Eastern Alps (Nonsberg–Ulten zone): geochronology and new petrological constraints. *Earth and Planetary Science Letters* 210, 509–26.
- Vaccaro C, Atzori P, Del Moro A, Oddone M, Traversa G and Villa IM** (1991) Geochronology and Sr isotope geochemistry of late-Hercynian dykes from Sardinia. *Schweizerische Mineralogische und Petrographische Mitteilungen* 71, 221–30.
- Vai GB** (1991) Palaeozoic strike-slip rift pulses and palaeogeography in the circum-Mediterranean Tethyan realm. *Palaeogeography, Palaeoclimatology, Palaeoecology* 87, 223–52.
- Veevers JJ** (1989) Middle/Late Triassic (230±5 Ma) singularity in the stratigraphic and magmatic history of the Pangean heat anomaly. *Geology* 17, 784–87.
- Visonà D** (1997) The Predazzo multipulse intrusive body (Western Dolomites, Italy). Field and mineralogical studies. *Memorie della Società Geologica Italiana* 49, 117–25.
- Visonà D and Zanferrari A** (2000) Some constraints on geochemical features in the Triassic mantle of the easternmost Austroalpine-Southalpine domain: evidence from the Karawanken pluton (Carinthia, Austria). *International Journal of Earth Science* 89, 40–51.
- von Raumer, JF** (1998) The Palaeozoic evolution in the Alps: from Gondwana to Pangea. *Geologische Rundschau* 87, 407–35.
- Woolley AR, Bergman SC, Edgar AD, Le Bas MJ, Mitchell RH, Rock NMS and Scott-Smith BH** (1996) Classification of lamprophyres, lamproites, kimberlites, and the kalsilitic, melilitic, and leucitic rocks. *Canadian Mineralogist* 34, 175–86.
- Zanetti A, Mazzucchelli M, Rivalenti G and Vannucci R** (1999) The Finero phlogopite-peridotite massif: an example of subduction-related metasomatism. *Contribution to Mineralogy and Petrology*, 134, 107–22.
- Zanetti A, Mazzucchelli M, Sinigoi S, Giovanardi T, Peressini G and Fanning M** (2013) SHRIMP U–Pb zircon Triassic intrusion age of the Finero mafic complex (Ivrea-Verbano zone, Western Alps) and its geodynamic implications. *Journal of Petrology* 54, 2235–65.
- Ziegler PA and Stampfli GM** (2001) Late Paleozoic–Early Mesozoic plate boundary reorganization: collapse of the Variscan Orogen and opening of the Neotethys. *Natura Bresciana, Annali del Museo di Scienze Naturali* 25, 17–34.